HOSTED BY

ELSEVIER

Contents lists available at ScienceDirect

Saudi Pharmaceutical Journal

journal homepage: www.sciencedirect.com

Identification of antidiabetic inhibitors from *Allophylus villosus* and *Mycetia sinensis* by targeting α-glucosidase and PPAR-γ: *In-vitro*, *in-vivo*, and computational evidence

Md Nur Kabidul Azam [a], Partha Biswas [a,b], Md. Mohaimenul Islam Tareq [a], Md Ridoy Hossain [a], Shabana Bibi [c,d], Md. Anisul Hoque [a], Amia khandker [e], Md Ashraful Alam [f], Md. Nazmul Hasan Zilani [g], Mohammad Shahedur Rahman [h], Norah A. Albekairi [i], Abdulrahman Alshammari [i], Md. Nazmul Hasan [a,*]

[a] *Laboratory of Pharmaceutical Biotechnology and Bioinformatics, Department of Genetic Engineering and Biotechnology, Jashore University of Science and Technology, Jashore 7408, Bangladesh*
[b] *ABEx Bio-Research Center, East Azampur, Dhaka 1230, Bangladesh*
[c] *Department of Biosciences, Shifa Tameer-e-Millat University, Islamabad 41000, Pakistan*
[d] *Yunnan Herbal Laboratory, College of Ecology and Environmental Sciences, Yunnan University, Kunming 650091, China*
[e] *Biotechnology division, TechB Nutrigenomics, Dhanmondi, Dhaka 1209, Bangladesh*
[f] *School of Chemical Engineering, Zhengzhou University, Zhengzhou 450001, Henan, China*
[g] *Department of Pharmacy, Faculty of Biological Science and Technology, Jashore University of Science and Technology, Jashore 7408, Bangladesh*
[h] *Bioresources Technology & Industrial Biotechnology Laboratory, Department of Biotechnology and Genetic Engineering, Jahangirnagar University, Savar, Dhaka 1342, Bangladesh*
[i] *Department of Pharmacology and Toxicology, College of Pharmacy, King Saud University, Post Box 2455, Riyadh, 11451, Saudi Arabia*

ARTICLE INFO

Keywords:
Diabetes
Phyto chemical
Bioactivities
GC–Ms
Mycetia sinensis
Allophylus villosus
Computer-aided drug discovery

ABSTRACT

Diabetes mellitus (DM) is a metabolic disorder arising from insulin deficiency and defectiveness of the insulin receptor functioning on transcription factor where the body loses control to regulate glucose metabolism in β-cells, pancreatic and liver tissues to homeostat glucose level. Mainstream medicines used for DM are incapable of restoring normal glucose homeostasis and have side effects where medicinal plant-derived medicine administrations have been claimed to cure diabetes or at least alleviate the significant symptoms and progression of the disease by the traditional practitioners. This study focused on screening phytocompounds and their pharmacological effects on anti-hyperglycemia on Swiss Albino mice of n-hexane, ethyl acetate, and ethanol extract of both plants *Mycetia sinensis* and *Allophylus villosus* as well as the in-silico investigations. Qualitative screening of phytochemicals and total phenolic and flavonoid content estimation were performed significantly in vitro analysis. FTIR and GC–MS analysis précised the functional groups and phytochemical investigations where FTIR scanned 14, 23 & 17 peaks in n-hexane, ethyl acetate, and ethanol extracts of *Mycetia sinensis* whereas the n-hexane, ethyl acetate, and ethanol extracts of *Allophylus villosus* scanned 11 peaks, 18 peaks, and 29 peaks, respectively. In GC–MS, 24 chemicals were identified in *Mycetia sinensis* extracts, whereas 19 were identified in *Allophylus villosus* extracts. Moreover, both plants' ethyl acetate and ethanol fractioned extracts were reported significantly ($p < 0.05$) with concentrations of 250 mg and 500 mg on mice for oral glucose tolerance test, serum creatinine test and serum alkaline phosphatase test. In In silico study, a molecular docking study was done on these 43 phytocompounds identified from *Mycetia sinensis and Allophylus villosus* to identify their binding affinity to the target Alpha Glucosidase (AG) and Peroxisome proliferator-activated receptor gamma protein (PPARG). Therefore, ADMET (absorption, distribution, metabolism, excretion, and toxicity) analysis, quantum mechanics-based DFT (density-functional theory), and molecular dynamics simulation were done to assess the effectiveness of the selected phytocompounds. According to the results, phytocompounds such as 2,4-Dit-butyl phenyl 5-hydroxypentanoate and Diazo acetic acid (1S,2S,5R)-2-isopropyl-5-methylcyclohexyl obtained from *Mycetia sinensis* and *Allophylus villosus* extract possess excellent antidiabetic activities.

* Corresponding author.
E-mail address: mn.hasan@just.edu.bd (Md. Nazmul Hasan).

https://doi.org/10.1016/j.jsps.2023.101884
Received 27 August 2023; Accepted 23 November 2023
Available online 25 November 2023

1. Introduction

Diabetes is a chronic and preventable disease. Insufficient insulin production or impaired insulin utilization are the causes of diabetes mellitus, identified as a chronic disease by optimized blood glucose levels. Uncontrolled blood glucose can result in hyperglycaemia, which can cause severe damage to various body systems, including nerves and blood vessels (Barrett-Connor, 2003). Genetic and environmental factors influence hyperglycemia, impeding insulin secretion, and resistance in type 2 diabetes mellitus (T2DM) (Pal & McCarthy, 2013; Paramasivam et al., 2016). According to the Global Burden of Disease Collaborative Network, diabetes causes more than one and a half million deaths worldwide every year and significantly impacts cardiovascular health and kidney disease (Roth, 2018). Approximately 530 million adults aged 20 to 79 years and 135.6 million among the aged 65–99 years worldwide (Gamboa-Antiñolo, 2023) are affected with diabetes. International Diabetes federation ranked Bangladesh as number 9 for the 20 to 79 years aged people suffering from diabetes without a diagnosis in 180 countries. According to WHO reports, 2 million diabetics have died from diabetes and its complications. From 2000 to 2016, total 7,108,145 deaths were reported in the 108 selected countries (Ling et al., 2020) were related to diabetes. It has been estimated that global health expenditure on diabetes compared with US$760 billion in 2019 to reach US$825 billion by 2030 and US$845 billion by 2045 (Chowdhury et al., 2022).

There is evidence that single nucleotide polymorphisms (SNPs) within the PPARG gene, a nuclear receptor, can regulate lipid and glucose metabolism in the body (Sarhangi et al., 2020). Peroxisome proliferator-activated receptor-gamma performs the insulin action by increasing the tissue's sensibility (muscle, adiposity tissue, and liver) (Bermúdez et al., 2010) with the metabolic activities of glucose uptake in skeletal muscle and adipose tissue and lowering hepatic glucose production (Derosa & Maffioli, 2012). α-glucosidase inhibitors (AGIs) have also emerged as a prominent class of drugs that slow down carbohydrate metabolism and control blood glucose levels after meals (Sathish Kumar & Bhaskara Rao, 2016). α-glucosidase inhibitors (AGIs) perform significant glycaemic control and adjust insulin levels (Van de Laar et al., 2005b), which has not noticed any effect on mortality and morbidity (van de Laar et al., 2005a). Nowadays, α-glucosidase inhibitors and Peroxisome proliferator-activated receptor-gamma inhibitors are used as anti-diabetic drugs for glycaemic control and insulin homeostasis. Researchers have demonstrated strong evidence of phytochemicals' ability to target the PPAR-γ nuclear receptor, as well as acting as glucosidase inhibitors and modulating other genes involved in controlling blood glucose (Florez et al., 2007; Mahnashi et al., 2022; Tiji et al., 2021). Furthermore, bioactive compounds found in plants, including polyphenols and secondary metabolites, have been shown to modulate nucleotide chains and influence gene expression, thus contributing to preventing and treating type II diabetes as well as its complications (Felisbino et al., 2021).

Phytochemicals, also known as phytonutrients, are crucial to drug development for chronic diseases (Murugan et al., 2021; Singh et al., 2016), utilizing their bioactivity to prevent and treat illnesses (Lila & Raskin, 2005). In fact, approximately 80 percent of the global population relies upon phytochemical-based medicines (Ekor, 2014; Kelly et al., 2005), which have become the most significant source of modern pharmaceutical industries (Kumar & Egbuna, 2019). The United States has recently reported that 25 % of medical prescriptions are phytochemical-based (Azam et al., 2022). The World Health Organization (WHO) recognizes the importance of phytochemicals derived from more than 80,000 plant species, which offer effective treatment options with minimal side effects for chronic and acute diseases (Bhat, 2021b; Dev, 1997). 121 pharmaceutical products formulated with phytochemicals have emerged worldwide in the last century, based on traditional knowledge systems from 2800 BCE (Pan et al., 2014).

There are several indigenous communities in Bangladesh. One of them is the Chakma community, which mainly lives in Rangamati; Chittagong hill track districts, Bangladesh, and has its own culture, language, and medicinal practices (Rahmatullah et al., 2012b). The Chakma community has long recognized the prevalence of diabetes, so practitioners have relied on two significant plants (local Chakma names) known as Soy demi and Tin Shingha Pada to treat the disease, claiming they can provide significant relief or even cure it entirely; especially traditional practitioners of Sapchari, Gagra, Rangamati. *Mycetia sinensis*, initially identified in 2009 from Moulavi Bazaar National Park in Bangladesh, reported by Bangladesh National Herbarium, belongs to the Rubiaceae family with 45 species worldwide (Yan et al., 2016). The plant's native habitat is South China, which is usually grown in the tropical wet biome, and it has also been in the streamside at the Sapchari area of the Rangamati hill track district. Moreover, there are 255 species in the Sapindaceae family, including *Allophylus villosus*, which is found worldwide and grows mainly as a shrub in tropical wet areas (Chavan & Gaikwad, 2016). It was discovered in a wet tropical region in the Sapchari area of the Rangamati hill track district, commonly known as Tin Sangha Pada. Despite this, the medicinal properties of these plants remain unknown. In the search for a new phytochemical source for developing diabetes mellitus drugs, our research focused on *Mycetia sinensis* and *Allophylus villosus*. *Mycetia sinensis* is traditionally used for uncontrolled urination, a weakness for adults, and Meho (for young people). The other plant, *Allophylus villosus* traditionally used for Menorrhagia (Women), Dysentery (for cattle), debility (for young), jaundice, and Diabetes.

In light of significant studies on the bioactivities of *M. sinensis* and *A. villosus*, research focused on nutrigenomic approaches or computer-aided drug development to identify and design potential drug candidates derived from these plant extracts (Baehaki et al., 2020a; Karim et al., 2020a; Simorangkir et al., 2019). Using these approaches, the existing phytochemicals in these plants have been optimized, and therapeutic properties to treat diabetes have been enhanced. Computer-aided drug designing (CADD) analysis can hasten the drug development process by screening large compounds to predict their toxicity and select them as lead compounds (Gazor et al., 2017; Grover et al., 2003a; Küme et al., 2018). For identification of possible active conformation, binding affinity strain discipline associated with the binding mechanism has been performed by Quantum mechanics (Socrates, 2004) and Molecular docking to detect binding affinity and interaction between protein and ligand molecules (Grant-Peters et al., 2022; Saha et al., 2022). It also identifies potential drug candidates for whom further analyses have been done by Molecular Dynamics Simulation (MDS). Molecular Dynamics Simulation is a strong enough method to justify protein–ligand interactions with an artificially created environment that imitates the human body (Simorangkir et al., 2019).

We aimed to identify the active phytochemicals for treating diabetes mellitus from *M. sinensis* and *A. villosus*. The study has been focused on In-house content determination of anti-oxidant, functional group screening, Phytochemical identification by GC–MS with observation of bioactivities (Mihailović et al., 2021; Ramírez-Alarcón et al., 2021). Finally, the phytocompounds obtained from *Mycetia sinensis* and *Allophylus villosus* are evaluated in order to identify active phytochemical as novel drug candidates targeting alpha glucosides and Peroxisome proliferator-activated receptor gamma for inhibition activities to treat diabetes by in-vivo, in-vitro and in silico approaches.

2. Methods and materials

2.1. Plant materials

Aerial parts of *Mycetia sinensis* and leaves *Allophylus villosus* were collected from the Hill slope, stream side and wet tropical biome of Sapchori, Manikchori, Ghagra, Rangamati Hill track District, Bangladesh (geographically sated as the Latitude: $22^0 66'$ and Longitude: $92^0 08'$) during the rainy season of 2019 with the support of Rangamati

Development Board, GORBA Tourism and Local Chakma folk medicinal Practitioners. Nearly 6 kg of *M. sinensis* and 8 kg of *A. villosus*, green leaves were collected for this research work. Herbarium sheets for *A. villosus* and *M. sinensis* were prepared for identification and Certification, which were authenticated as *Mycetia sinensis* (Hemsl.) Craib (DACB Accession Number:54906) and *Allophylus Villosus* (Rob.) Blume (DACB Accession Number: 54909) by Dr. Mahbuba Sultana, Senior Scientific Officer (Deputation), Associate Professor (Botany), Bangladesh National Herbarium, Ministry of Environment, Forest and Climate Change, Chiriakhana Road, Mirpur-1, Dhaka-1216.

2.2. Extract preparation

Dried aerial parts and leaves are grinded (Capacitor start motor, Wuhu motor, Made in China) into grainy powder at the Laboratory of Pharmaceutical Biotechnology & Bioinformatics, Jashore University of Science and Technology. Coarse powder of *M. sinensis* (750 g) and *A. Villosus* (600 g) were macerated in respectively 5 Jars and 4 jars (150 g powder in each jar) by multilevel maceration using hexane (nonpolar), ethyl acetate (semipolar), and 98 % ethanol (polar) solvents (Baehaki et al., 2020b). 300 ml of n-Hexane solvent (Daejung chemicals, lot no: H3243SH1) were used for maceration in each jar, filtered twice by 110 mm Whatman Filter paper (cat no: 1001110) from GE Healthcare and the filtrates obtained were concentrated on the rotary evaporator (RE-100 PRO, DLAB Scientific Inc., China) vacuum maintaining temperature 40 °C with 40 RPM to get concentrated n-hexane extracts at Central Laboratory, Department of Biotechnology, Jashore University of Science & Technology, Bangladesh.

The pulp portions of each plant were macerated with ethyl acetate (Daejung chemicals, lot no: E3180TF1) solvent (400 ml in each jar), filtered twice, and the filtrate poured was concentrated to procure concentrated ethyl acetate extract. Furthermore, the pulp portion was re-macerated with 98 % ethanol (EMSURE r, Merck KGaA, Index number: 603–002-00–5) solvent, filtered twice, and the filtrate procured was concentrated to procure concentrated ethanol extract (Simorangkir et al., 2019). A piece maceration process for several solvents lasts for 8 days 24 h, with thrice stirrers in a day (Asmilia et al., 2020). The extraction results produced a yield of a fraction of extract n-hexane, ethyl acetate & ethanol of apiece plant *M, sinensis,* and *A. villosus*, and extracts were collected in glass vials. Fractioned extracts of n-hexane, ethyl acetate, and ethanol from *M. sinensis* were labelled as M_N, M_EA, M_E, and *A.villosus* were labelled respectively A_N, A_EA, A_E and accumulated at 4∘C temperature for further experimental uses.

2.3. Total phenolic content

The total polyphenol content of six extracts was ascertained by the modified Folin-Ciocalteu method (Rahman et al., 2021). Equal fractional parts of 0.5 ml extract from each solution (1 mg/mL) of six extracts and standard (1 mg/mL) were mixed properly with 5 ml of 1:10 (v/v) FC reagent. As per protocol, 4 ml of sodium carbonate (7.5 % w/v) was added up to the mixture. After vortex for 15 s, Sample mixtures were incubated with a thermostat at 40 °C for 30 min. The UV filter was 765 nm. Different concentrations (0–50 μg/ml) of Gallic acid were used for standard curve generation, ($y = mx + c$). Total Phenolic Content was measured by the equation as TPC; A= (C*V)/M (mg/g).

2.4. Total flavonoid content

Total flavonoid content in selected plant extracts was determined using 200 μ l $AlCl_3$ (1 %) and 200 μ l potassium acetate (CH_3CO_2K) (1 M) with 1 ml solution of extract or standard solution (1 mg/mL) in the modified colorimetric methods from existing researches (Karim et al., 2020b). The results were derived from the calibration curve ($y = mx + c$) of Quercetin (0–50 μg/mL), and expression of Quercetin Equivalents (QE) was ascertained (mg/ml) from the calibration line and in terms of Quercetin Equivalent dry extract in per gram for six extracts. Total Phenolic Content TPC; A= (C*V)/M (mg/gm).

2.5. Fourier transforms infrared (FTIR) spectroscopy

Fourier transform infrared (FTIR) spectra were set down using an FTIR spectrophotometer (IR prestige- 21, Shimadzu) at Wazed Mia Science Research Center, Jahangir Nagar University, Saver, Dhaka. All six extracts of *M. sinensis* & *A. villosus,* respectively, n-hexane, ethyl acetate, and ethanol solvent, were thoroughly mixed in a ratio of 1:100 with an infrared transparent matrix or carrier (potassium bromide). KBr mixture powder was compressed at 6-ton pressure in a hydraulic press (Shimadzu, Japan) for 5 min for KBr disk preparation (Saifuddin et al., 2017). The prepared disc for each extract was scanned at the resolution 4 (1/cm), from 4000to 500 with Happ- Genzel Apodization, and observed eleven scanned peaks for the extract A_N, Thirty-Five for A_EA, Twenty Nine for A_E, Fourteen for M_N, Twenty-Three for M_EA and Eighteen Scanned peak for M_E. Functional groups were sorted out from the IR Spectrum Table and Chart of Sigma-Aldrich (Socrates, 2004) for natural products and Insta NANO FTIR database software (Grant-Peters et al., 2022).

2.6. Gas Chromatography & Gas Chromatography -mass spectrometry (GC & GCMS)

Gas Chromatography for each fractioned extract from *A. villosus* and *M. sinensis* were performed with Restek 30 m X 0.25mmID X 0.25 um Cat#14623 column, using Helium gas as mobile phase at 4.5 flow rate, Detection method: FID; temperature 250 °C; Range: Bipolar, 10000 mV, 25 Samp. Per Sec at Analytical Laboratory, Wazed Mia Science Research Centre, Jahangirnagar University, Saver, Bangladesh. After analyzing Gas Chromatogram from all selected extract of A. *villosus* and *M. sinensis*, we investigated GC–MS from a potential fractioned extract from *A. villosus* and *M. sinensis*.

Ethyl acetate and ethanol extracts as the potential extracts from *A. villosus* and *M. sinensis* were performed GC–MS analysis on Agilent 7000DGC/QT triple quadrupole GC/MS analyzer using Mass Hunter software for compound identification at the School of Chemical Engineering, Zhengzhou University, China. N-hexane fractioned has skipped due to no peaks performed in GC analysis, which was conducted before GC–MS for all fractioned extracts of *A. villosus* and *M. sinensis*. GC–MS method was developed in-house (Bharat et al., 2017) where Gas Chromatograph (Agilent, USA 8890) with an i.d. (30 m x 0.25 mm) and 0.5 um film thickness capillary column HP-5 ms (Agilent USA, Serial no: T562436H) was used at f scan mode (total) and split ratio 1:20 (split injector mode was), Mass Selective Detector (MSD) was 5977C single quadrupole, injector temperature 220^0 interface temperature 230^0 and the injection volume was 1ul in GC–MS. As the carrier gas was Helium at 60 Kpa pressure, 1 ml/min flow rate. Mass spectra were detected at 70 eV. The programmed temperature was as follows: column temperature was started from 60 °C (2 min holding) and linearly increased by 5 °C/min to 130 °C (2 min holding); after that, it was raised by 4 °C/min to 200 °C (2 min holding); further, it was increased by 8 °C/ min. to 250 °C (10 min holding). Total GC run time was 55 min.

2.7. Animal preparation

Two sets of young Swiss-albino mice (70 mice in each set) aged 4–5 weeks were procured from the Animal Research Division of the International Centre for Diarrhoeal Disease and Research, Bangladesh (ICDDR, B). Set one, average weight 22–26 g, was used for the OGTT experiment, and set number two, average weight 25–29 g, was used respectively for the observation of Serum creatinine and alkaline phosphatase in the same experiment. All animal biosafety and care protocols were in accordance with as well as approved by the university ethical committee. Mice were kept at a controlled humidity (50–70 %),

temperature 25 ± 1 °C, and Photo period of 12 h/12/h (light and dark cycle) in the animal house of Jashore University of Science and technology for 10 days adaptation period after purchasing. During the adaptation period, mice were fed a pallet diet, cucumber, and water as their pleasure. In our research study, we used all the research animals after getting the ethical approval certificate from the Ethical Review Committee, Faculty of Biological Science and Technology, Jashore University of Science and Technology, Jashore-7408, Bangladesh (Ethical Approval Reference Number: ERC/FBST/JUST/2022–111; Date: 13th February 2022).

2.8. Oral glucose tolerance test

Animals were modelled in 14 groups with group average weight 116–119 g (5 mice in each group) from Set One. For the oral glucose tolerance test (OGTT) assessment, all groups were fasted overnight (13 h). The control group received only DW during gavaging, and the Standard group received standard Glibenclamide (Commercial name Dibenol) 5 mg/kg orally. Group A and Group B were treated with extract of *Mycetia sinensis* n-Hexane (M_N) respectively by the dose of 250 mg/kg and 500 mg/kg body weight. Group C and Group D were treated with respectively the dose of 250 mg/kg and 500 mg/kg body weight of *M. sinensis* Ethyl acetate (M_EA) extract; accordingly, Group E (250 mg/kg) and Group F (500 mg/Kg) were treated with extract of *M. sinensis* Ethanol (M_E), Group G (250 mg/kg) & Group H (500 mg/kg) were treated with *A. Villosus* n-Hexane A_N) Extract, Group I (250 mg/kg), and Group J (500 mg/kg) were treated with *A. villosus* Ethyl Acetate (A_EA) extract. Group K & Group L were treated with *Allophylus Villosus* Ethanol (A_E) in doses respectively 250 mg/kg & 500 mg/kg body weight. After 30 min of gavaging of extracts & a standard dose of glucose (3 kg/kg body weight) was administrated orally. After 0,30,60 and 90 mins of a glucose load, collected blood samples from the caudal vein of mice and blood glucose levels were analysed by commercially available blood glucose test strip from One call plus as well as using a glucometer of one call plus (Designed by ACON Labs USA, made in China).

2.9. Serum creatinine & alkaline phosphatase test

Animals were modeled in 14 groups with D and were treated with respectively the dose of 500 mg/kg and 250 mg/kg body weight of *Allophylus* average age 127–133 gm (5 mice in each group) from Set Two. For Assessment of Serum Creatinine, all groups were fasted overnight (15 h). The control group was treated only DW during gavaging, and the Standard Group received oral standard Glibenclamide (Commercial name Dibenol) 5 mg/kg. Group A and Group B were treated with extract of *Allophylus Villosus* n-Hexane A_N) respectively, by the dose of 500 mg/kg and 250 mg/kg body weight. Group C and Group D with *A. Villosus* Ethyl Acetate (A_EA) extract; accordingly, Group E (500 mg/kg) and Group F (250 mg/Kg) were treated with extract of *Allophylus Villosus* Ethanol (A_E), Group G (500 mg/kg) & Group H (250 mg/kg) were treated with *Mycetia sinensis* n-Hexane (M_N) Extract, Group I (500 mg/kg) and Group J (250 mg/kg) were treated with *Mycetia sinensis* Ethyl acetate (M_EA) extract. Group K & Group L were treated with *Mycetia sinensis* Ethanol (M_E) in the dose respectively 500 mg/kg & 250 mg/kg body weight. Glucose (3 kg/kg body weight) was administrated orally after 30 min of gavaging of extracts & standard. After 120 mins of a glucose load, (Ketamine/Xylazine for anaesthesia. 0.1 ml/ 20gm IP dosage were administrated), blood samples were collected in a fresh vial from a heart puncher (Rahmatullah et al., 2012a), and serum was separated by centrifugation (4000 rpm for 15 min) (Grover et al., 2003b). Serum creatinine was measured using a commercial kit (Cromatest creatinine kit) following the Jaffe method (Küme et al., 2018) by the Spectrophotometer (Ryto 9200 semi-auto analyzer at Health Garden Diagnostic Centre) with 510 nm wavelength. From the same serum source, Alkaline phosphatase was measured using a commercial kit (Cromatest Alkaline Phosphatase kit) according to DGKC method (Gazor et al., 2017) by Spectrophotometer (Ryto 9200 semi-auto analyser at Health Garden Diagnostic Centre) with 405 nm wavelength.

2.10. Computational analysis

2.10.1. Retrieval of phytocompounds and preparation

A final library of 43 phytocompounds was retrieved through GC–MS study of two separate extracts of two selected plants. The separated phytocompounds, as well as the control drug, isolated from PubChem database (https://pubchem.ncbi.nlm.nih.gov/, accessed on the 26th of April 2023) in SDF (spatial data file) format including tertiary 3D structures. Using the LigPrep panel of the Maestro Application, Schrödinger Suite Software (https://www.Schrödinger.com/products/maestro), the structures of all ligands were prepared. Utilizing the OPLS3e force field and the Epik ionizer, the minimization process is carried out at a typical P^H range of 7.0 to (+/-2.0), having an RMSD of 1.0 and 32 conformers at most of the structure.

2.10.2. Pharmacokinetics analysis of phytocompounds

Several pharmacokinetic parameters of druggable molecules like the experimental agonists, including absorption, distribution, metabolism, excretion as well as toxicity, are predicted by using ADME/T to check ADME parameters; every 43 ligands have been run through into the Swiss ADME server (http://www.swiss.adme.ch/). After that, six ligands out of the 43 ligands were subjected to toxicity characterization only because those six substituents did not violate the Lipinski principle. Using web-based technology, several putative antagonists' toxicity was probed through 'pkCSM' (http://biosig.unimelb.edu.au/pkcsm/prediction) server. Six compounds were ultimately selected to undergo additional computerized research as well as investigations.

2.10.3. Ligand activity prediction by QSAR analysis

The biological activity of the 6 phytochemicals was contrasted by implementing the renowned server PASS (Prediction of Activity Spectra for Substances) (http://www.way2drug.com/passonline) that forecasts results depending on a substance's structural makeup (Ban et al., 2018). The possibility that a particular substance will be a member of that substance's inactive and active subgroups is predicted using the Structure-Activity Relationship Base (SAR Base). The input was given in SMILES (Simplified Molecular Input Line Entry System) format for the phytochemicals structure. The Pi (probable inactivity) and Pa (probable activity) were determined for each ligand. Consequently, only activities involving diabetes were taken into account (Roos et al., 2019).

2.10.4. Calculation of quantum mechanics

The conformational study of ligands within the protein's binding site is essential for understanding their active conformation, binding affinity, and strain discipline. To achieve this, a systematic approach is adopted that integrates computational modelling and simulation techniques. Results and Discussion emphasize the importance of conformational studies in understanding the active conformation and binding affinity of ligands. However, the presence of metal ions in ligand–protein complex systems impedes accurate descriptions using traditional molecular mechanics (MM) techniques (Friesner & Guallar, 2005). To address these challenges, advancements in computational models are needed. The ligand was minimized using Jaguar v-10.9's QM (quantum machinal) calculation, which employed the density functional theory (DFT) (Lu et al., 2016). B3LYP (Becke exchange functional) (Becke, 1988), which integrated 6–31 G (d,p) basis sets with Lee, Yang, and Parrs (LYP) (Lee et al., 1988), was used to execute the DFT. For this reason, we proceeded to perform DFT or QM calculations. Within the DFT calculation framework, our focus was on analyzing the frontier molecular orbitals, particularly the lowest unoccupied molecular orbitals (LUMOs) and highest molecular orbitals (HUMOs), as well as energy gap between them. While the LUMO's energies imply the molecule's capability to take electrons from the protein, the HOMO's energy

values provide insights into the ligand molecule's ability to give electrons. So, the frontier energies (ε) of LUMOs and HOMOs were used to determine the hardness and softness of the chosen compounds. In particular, the Koopmans theorem equation and the Parr and Pearson interpretation were used to quantify the softness (s) and hardness (η) of the drugs (Parr, 1980; Pearson, 1986). The concept of hardness in chemistry refers to an atom's resistance to charge transfer to another atom or metal surface, while softness represents the atom's ability to accept electrons. The chemical hardness can be calculated using all Equations, where I denote the ionization potential ($-E_{HOMO}$), A represents the electron affinity ($-E_{LUMO}$). A smaller value of hardness indicates greater reactivity, while a larger value signifies lower reactivity. Conversely, softness (S) measures the atom's capacity to receive electrons, and it is inversely related to hardness. The parameter η represents the hardness. These equations provide a quantitative measure of reactivity and electron acceptance capabilities for atoms and molecules, offering valuable insights in chemical analysis and understanding. To create various sensitivity indices, several subsequent formulae have been utilized:

$$E_g = E_{LUMO} - E_{HOMO}$$

$$IP = -E_{HOMO}$$

$$EA = -E_{LUMO}$$

$$\eta = \frac{(E_{LUMO} - E_{HOMO})}{2}$$

$$\mu = \frac{(E_{LUMO} + E_{HOMO})}{2}$$

$$S = \frac{1}{\eta}$$

The ionization potential (E_{HOMO}) is referred to in Equation and stands for electron affinity (E_{LUMO}). The equation described above states that greater reactivity results from a lower hardness value and vice versa. As opposed to S, this measures an atom's capacity to accept electrons, and η, which measures toughness.

2.10.5. Optimization of targeted protein and generation of receptor grid

The RCSB protein data bank (PDB) (https://www.rcsb.org/, accessed on 27 October 2022) was used to retrieve the target protein in 3D format. The target protein structure (PDB ID: 8B8Z and 3WY1) is used as a receptor in molecular docking analysis (Biswas et al., 2023a;Jabin et al.,2023; Shiau et al., 1998). After the file has been downloaded, the Protein Preparation Wizard 12.5 that is included with the Maestro Application (Schrödinger 2020–3 Schrödinger, LLC, New York, NY, USA, 2020) was utilized in order to carry out the process of preparing the protein. Prime has been selected for use in producing disulfide bonds, generating zero-order bonds to metals, developing disulfide bonds, and completing any remaining side chains and loops. In addition to making use of the set cap termini and excluding waters having a temperature greater than 5 then the heat groups, we additionally conducted the Epic application (Schrödinger Release version 2020–3), which was executed to produce thermal states with pH values ranging from 7.0 to 2.0 (Al Azad et al., 2022; Ferdausi et al., 2022; Hasibuzzaman et al., 2023; Sohel et al., 2023). At a pH level of 7.0, the hydrogen bond was found in PROPKA, and the degradation was stopped at an RMSD of 0.30 by limiting the exposure of heavy atoms with the use of the refine tab and the OPLS3e force field. Subsequently, the receptor grid was produced by centering attention on the active site's point provided by the protein's endogenous ligand.

2.10.6. Site-Specific super molecular docking

Maestro (Schrödinger Release 2021–2: Maestro, Schrödinger, LLC, New York, NY, USA, 2023) was employed in the XP program, which represents "extra precision "site-precision XP (extra precision) molecular docking analysis. Afterward completing XP (extra precision) molecular docking analysis via Schrödinger Suite Software's Maestro tool (https://www.Schrödinger.com/products/maestro), the PDB format of each protein–ligand complex was obtained from post-viewing files of molecular docking trajectories. Finally, these protein–ligand compound complexes were used for post-docking data visualization analysis to study the non-bond interactions and measure their hydrophobic properties and bioactivity (Biswas et al., 2022b; Dey et al., 2022a; Dey et al., 2022b; Khan et al., 2021).

2.10.7. Post-Docking visualization

After conducting the site-specific XP (extra precision) molecular docking analysis by Schrödinger Release 2021–2: Maestro, Schrödinger, LLC, New York, NY,2020–3), the combined PDB format of the targeted protein and selected ligand compounds were extracted for post-docking analysis (Arefin et al., 2021; Rahman et al., 2020b). The non-covalent interactions (Hydrogen and Hydrophobic bonds) among the receptor-ligand structural complexes were identified through Ligplot + version 2.2. The visualization tool is excellent due to the Java interface (Java SE Runtime Environment 8u271), which only permitted concatenated PDB files produced by the Maestro application. Additionally, the structural binding compactness, non-polar and polar interaction bonds in complexes, and other features were validated using Discovery Studio Visualizer 64-bit (http://media.accelrys.com/downloads/visualizer/45/DS45Client.exe).

2.10.8. Molecular dynamics simulation (MDS)

CID-6327703, CID-102506517, CID-441314(Control) and CID:605775, CID:605777, CID:15764573, CID:91720824, and CID:77999 (Control) were chosen as its two prospective ligand molecules in to be tested for their uniformity for interacting to the targeted Alpha Glucosidase (PDB ID: 3WY1) and Peroxisome proliferator-activated receptor gamma (PPARG) (PDB ID: 8B8Z) protein model respectively using 100 ns MD simulations for analyzing the thermodynamic compatibility of the protein–ligand complexes, Schrödinger "Desmond v3.6 Program" (https://www.Schrödinger.com/) (Paid version) had been used within a Linux framework for perform molecular dynamic simulations evaluating various protein–ligand complex structures. Using such a framework, the predefined TIP3P aqueous strategy to establish a predetermined volume contains a periodic bounding box shape with orthorhombic form divided through a space of 10 Å. Recommended ions, such as 0+ and 0.15 M salt (Na+ and Cl−), have been selected as well as dispersed at randomization across its chemical solvent environment to neutralize electric power in its structure. After building its solvency proteins structures containing agonist combinations, the system's framework subsequently reduced and comfortable utilizing the protocol that applied force field constants OPLS3e included inside the Desmond package. Every Isothermal-Isobaric ensemble (NPT) assembly which utilized overall Nose-Hoover temperatures combinations as well as its isotropic technique was contained around 300 K as well as one atmospheric pressure (1.01325 bar) as well as was followed by 50 PS grabbing pauses using an efficacy of 1.2 kcal/mol. The Simulation Interaction Diagram (SID) from the Desmond modules of Schrödinger Suite was used to assess the molecular dynamics simulation's fidelity. Molecular Surface area (MolSA), polar surface area (PSA), Solvent-accessible surface area (SASA), protein–ligand interactions (P-L) and intermolecular hydrogen bonds were utilized to evaluate the stability of this protein–ligand complex (Arman Sharif et al., 2023; Paul et al., 2022; Rahman et al., 2020a; Zilani et al., 2021).

2.10.8.1. Analysis of simulation trajectories. The Schrödinger Maestro application version 9.5 was used to produce the Molecular Dynamics Simulation images. The Simulations Interaction Diagram (SID) of the

Desmond modules in the Schrödinger was utilized to explore the prospective simulation scenario and assess the accuracy of the molecular dynamic's simulation. Molecular surface area (MolSA), polar surface area (PSA), root-mean square deviation (RMSD), protein–ligand contacts (P-L) and root-mean square fluctuation (RMSF) was used to constancy of the protein–ligand complex structure based on the trajectory effectiveness.

2.10.9. Post MDS thermal MMGBSA calculation

We utilized thermal_mmgbsa.py python package to approximate the free energies of the complexes during the 100 ns simulation time. The Desmond MD trajectory was divided into 20 individual frame pictures, which were then ran via MMGBSA and then extracted the ligand from the receptor.

3. Results

3.1. Total phenol content

Measured phenolic content for six extracts (M_N, M_EA, M_E, A_N, A_EA, A_E) were determined by using a standard calibration curve ($Y = 0.0054X + 0.0079$; $R^2 = 0.9936$) (Fig. S1**A**) and it was found to be the dry extract were 16.31481481 mg for *M. sinensis* n-Hexane (M_N), 36.31481481 mg *M. sinensis* ethyl acetate (M_EA) & 11.5926 ± 0.0926 mg *M. sinensis* ethanol (M_E); 30.2963 ± 0.093 mg in *A. villosus* n- Haxen (A_N), 45.7593 mg in *A. villosus* Ethyl Acetate (A_EA) and 483.3519 ± 4.4444 mg in *A. villosus* Ethanol (A_E) (Table 1) as gallic acid equivalents/g.

3.2. Total flavonoid contents

Total flavonoid contents were concluded from the linear equation of the quercetin standard curve ($Y= = 0.0074X - 0.0029$; $R^2 = 0.9879$) (Fig. S1**B**). Total flavonoid contents were obtained for each of six extracts of *M. sinensis* and *A. villosus* were 175.5271 ± 0.13514 mg in M_N, 40.324324 ± 0.06757 mg in M_EA, 83.2298 ± 0.00 mg in M_E, 176.946 ± 0.06757 mg in A_N, 167.014 ± 0.13514 mg in A_EA and 200.595 ± 0.06757 mg in A_E (Table 1).

3.3. Fourier transform infrared spectroscopy (FTIR)

FTIR spectra of six extracts from *M. sinensis* and *A. villosus* scanned number of peaks where *M. sinensis* N hexane (M_N) extract scanned 14 peaks with the area **Table S1 (a)** respectively extract of *M. sinensis* Ethyl acetate (M_EA) scanned 23 peaks **Table S1 (b)**, *M. sinensis* ethanol (M_E) scanned 18 peaks **Table S1 (c)**, *A. villosus* N-hexane (A_N) scanned 11 peaks **Table S1 (d)**, *A. villosus* Ethyl Acetate (A_EA) scanned 35 peaks **Table S1 (e)** and *A. villosus* Ethanol (A_E) scanned 29 peaks with the area **Table S1 (f)**. Estimated functional groups were evaluated from IR Spectrum Table and chart for organic compounds (Socrates, 2004). All the scanned peaks have plotted weave lengths in six graphical images (Fig. S2**a-f**).

Table 1
Total phenol and flavonoid content mg/g.

Plant Name	Solvent	Extract name	Total Phenolic Content mg/g	Total Flavonoid Content mg/g
Mycetia sinensis	n-Haxen	M_N	16.31481481 ± 0.00	175.5271 ± 0.13514
Mycetia sinensis	Ethyl Acetate	M_EA	36.31481481 ± 0.00	40.324324 ± 0.06757
Mycetia sinensis	Ethanol	M_E	11.5926 ± 0.0926	83.2298 ± 0.00
Allophylus Villosus	n-Haxen	A_N	30.2963 ± 0.093	176.946 ± 0.06757
Allophylus Villosus	Ethyl Acetate	A_EA	45.7593 ± 0.00	167.014 ± 0.13514
Allophylus Villosus	Ethanol	A_E	483.3519 ± 4.444	200.595 ± 0.06757

3.4. GC–MS

After performing Gas Chromatography, as the potential extract for GC–MS, ethyl acetate and ethanol extract from *A. villosus* and *M. sinensis* were resulted where n-hexane extracts from both plants *A. villosus* and *M. sinensis* have performed no peaks in GC analysis (**Figure S 3**).

In the GC–MS analysis of the Ethyl acetate extract of *M. sinensis* performed 23 peaks (Fig. 1**A**) which were analysed in MassHunter GC–MS peak area analysis & specified major compounds of the extract. Among these 23 peaks, the software, MassHunter LibSearch was unable to identify 12 compounds whereas it can be able to identify only 11 compounds with the names of compounds as well as Molecular Weight (MW), Molecular formula, Retention Time (RT) and area (%) of a compound. On the other hand, in a brief analysis by MassHunter LibSearch can be able to generate 3 extra retention times without peak area, indicating a poor number of minor compounds as well as it can identify the name, molecular weight and molecular formula of these 3 compounds. According to the name, molecular weight, molecular formula, area (%), and retention time of identified and unidentified compounds were illustrated in **Table S2 (a)** for Ethyl acetate extract of *M. sinensis*.

Ethanol extract of *M. sinensis* performed 10 peaks (Fig. 1**B**) in GC–MS analysis. All the peaks indicated the extract's primary compound, and LibSearch could identify their name, molecular weight, molecular formula, retention time, and area (%), which was depicted in **Table S2 (b)**.

Ethyl Acetate extract of *A. villosus* and Ethanol extract of *A. villosus* performed respectively 13 and 10 peaks (Fig. 1**C** and Fig. 1**D**) where LibSearch can able to identify all 13 compounds of Ethyl Acetate extract of *A. villosus* **Table S2 (c)** and 6 compounds **Table S2 (d)** of Ethanol extract of *A. villosus* with their name, molecular weight, molecular formula, retention time and area(%), rest of 4 compounds of Ethanol extract of *A. villosus* shows only retention time and area where the molecular name, molecular formula, molecular weight are still unknown to the LibSearch database of Agilent MassHunter analysis software for GCMS.

3.5. Oral glucose tolerance test

After administering different doses of six extracts in nondiabetic mice in 12 groups and a group was administrated standard drug for the oral glucose tolerance test (OGTT), Glucose was administrated orally 30 min later except control group. At the 0 min of a glucose load, the first cycle of blood glucose level was measured among the 14 groups, 2nd, 3rd, and 4th cycles of blood glucose level were monitored respectively after 30 min, 60 min, and 90 min of glucose administration and generated results in mmol/L (MEAN ± SD, n = 5) were described in Table 2, the statistical difference in blood glucose level was observed. Significant blood glucose reduction ($p \leq 0.05$) resulted at Grp C (M/EA 250 mg), Grp D (M/EA 500 mg), Grp E (M/E 250 mg) Grp F (M/E 500 mg); Grp G (A/N 250 mg); Grp I (A/EA 250 mg); Grp J (A/EA 500 mg); Grp K (A/E 250 mg); Grp L (A/E 500 mg) and Standard after 30 min of extract administration and during 0 min of glucose load, as compared to the mice receiving d/w (Control) **Table S3(a)**.

After 30 min, 60 min, and 90 min of glucose administration, statistical results of p-value, significant level, t statistics, and DF have been shown in **Table S3(b)**, **Table S3(c)**, and **Table S3(d)** respectively, as compared to the mice receiving d/w (Control).

After 30 min of glucose administration; statistical result according to significance level, p-value, DF, *t*-test generated as group A (*M. sinensis*, n-hexane extract 250 mg), Group F (*M. sinensis*, Ethanol extract 500 mg), Group H (*A. villosus*, n-hexane extract 500 mg), Group J (*A. villosus*, Ethyl acetate extract 500 mg), Group K (*A. villosus*, Ethanol extract 250 mg), and group L (*A. villosus*, Ethanol extract 500 mg), were insignificant as compared to control group. The rest of the 6 groups were significant

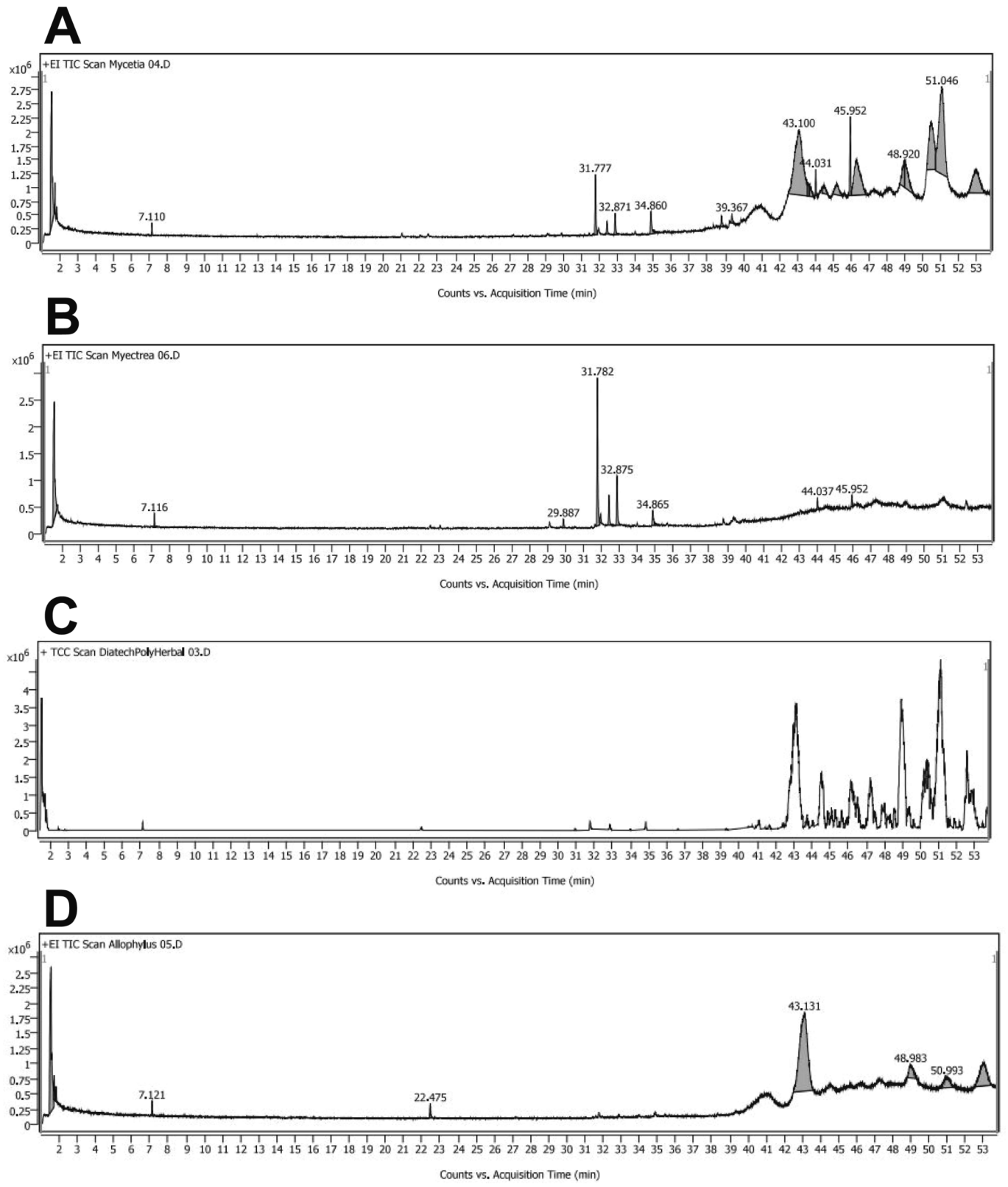

Fig. 1. GC–MS chromatogram figure **A**. Ethyl acetate extract of *Mycetia sinensis*; **B**. Ethanol extract of *Mycetia sinensis*; **C**. Ethyl acetate extract of *Allophylus villosus*; **D**. Ethanol extract of *Allophylus villosus.*

as compared with the control group, Group B; Group C; Group D, Group E, Group G & Group I ($p < 0.05$) as well as the standard group ($p < 0.001$) were significant After 60 min of glucose administration; statistical result according to significance level, p-value, DF, *t*-test was generated as the Group H (*A. villosus*, n-hexane extract 500 mg) and Group K (*A. villosus*, Ethanol extract 250 mg were insignificant as compared to the control group. The rest of the 10 groups ($p < 0.05$) and the standard group ($p < 0.001$) were significant as compared to the mice

Table 2
Level of blood glucose after 0 min, 30 min, 60 min, and 90 min of Oral glucose administration among the 13 groups as well as the control group on the basis of their mean ± SD.

Grp	Control	Grp Std	Grp A (M/N)	Grp B (M/N)	Grp C (M/EA)	Grp D (M/EA)	Grp E (M/E)	Grp F (M/E)	Grp G (A/N)	Grp H (A/N)	Grp I (A/EA)	Grp J (A/EA)	Grp K (A/E)	Grp L (A/E)
Time			250 mg	500 mg	250 mg	500 mg	250 mg	500 mg	250 mg	500 mg	250 mg	500 mg	250 mg	500 mg
0 min	10.18 ± 12.614	4.62 ± 1.355	8.76 ± 0.0.956	8.52 ± 0.2.153	6.98 ± 0.1.312	6.26 ± 0.871	6.18 ± 1.857	6.6 ± 1.309	6.86 ± 0.586	8.26 ± 2.128	7.32 ± 1.458	6.92 ± 1.006	6.62 ± 0.497	7.58 ± 1.668
30 min	12.64 ± 1.18	8.5 ± 3.907	11.04 ± 3.48	10.38 ± 2.58	8.38 ± 1.119	9.28 ± 3.065	10.3 ± 2.051	10.76 ± 3.28	10.04 ± 1.282	11.7 ± 3.965	8.7 ± 2.154	12.64 ± 1.924	13.52 ± 3.584	11.7 ± 1.646
60 min	11.02 ± 1.268	5.72 ± 1.303	8.72 ± 1.612	8.58 ± 1.602	7.9 ± 1.089	8.24 ± 2.802	7.86 ± 2.051	7.82 ± 1.413	7.68 ± 2.737	11.18 ± 3.704	8.98 ± 2.994	8.56 ± 1.024	10.42 ± 3.035	8.62 ± 1.672
90 min	9.64 ± 1.44	5.32 ± 1.112	9.44 ± 1.727	8.62 ± 1.758	7.5 ± 0.265	8.44 ± 1.864	5.34 ± 0.358	7.14 ± 1.791	7.7 ± 0.897	6.02 ± 1.117	8.84 ± 3.811	7.88 ± 0.77	7.58 ± 0.823	9.96 ± 2.177

During 0 min of glucose administration, the statistical result according to significance level, p-value ($p < 0.05$), DF, *t*-test generated as the group A (*M. Sinensis*, n-hexane extract 250 mg), Group B (*M. Sinensis*, n-hexane extract 500 mg) were insignificant as compared to the control group. The rest of the 10 groups ($p < 0.05$) as well as the standard group ($p < 0.001$) were significant.

receiving D/W (Control).

After 90 min of glucose administration; statistical results according to significance level, p-value, DF and *t*-test were generated as the Group A (*M. sinensis*, n-hexane extract 250 mg), Group B (*M. sinensis*, n-hexane extract 500 mg), Group D (*M. sinensis*, Ethyl acetate extract 500 mg), Group I (*A. villosus*, Ethyl acetate extract 250 mg) & Group L (*A. villosus*, Ethanol extract 500 mg) were insignificant as compared to the control group. The rest of the 7 groups ($p < 0.05$) as well as the standard group ($p < 0.001$) were significant as compared to the mice receiving D/W (Control).

3.6. Serum creatinine

After 30 min of extract administration glucose was orally administrated through all the groups except the control group. After 120 min of oral glucose administration, blood serum creatinine levels were measured and generated results described in Table 3. During the statistical analysis, considering in mg/dL, MEAN ± SD, n = 4 the p value shows that group D (*A. villosus*, Ethyl acetate,250 mg), Group F (*A. villosus*, Ethanol,250 mg), Group G (*M. sinensis*, n-hexane, 500 mg), Group H (*M. sinensis*, n-hexane,250 mg), Group I (*M. sinensis*, Ethyl Acetate, 500 mg) and Group J (*M. sinensis*, Ethyl Acetate, 250 mg) were significant ($p < 0.05$) as compared to the mice receiving d/w (Control).

3.7. Serum alkaline phosphatase

After 30 min of extract administration glucose was orally administrated through all the groups except the control group. After 120 min of oral glucose administration, blood serum alkaline phosphatase levels were measured and generated results described in Table 4. During the statistical analysis, considering in mg/dL, MEAN ± SD, n = 4, the p-value shows that Group B (*A. villous*, n-hexane) 250 mg/kg, Group I (*M. sinensis*, Ethyl Acetate) 500 mg, Group J (*M. sinensis*, Ethyl Acetate 250 mg, GRP K (*M. sinensis*, Ethanol) 500 mg, GRP L (*M. sinensis*, Ethanol) 250 mg were significant ($p < 0.001$) as compared to the mice receiving D/W (Control).

3.8. Findings of computational analysis

3.8.1. Construction of a ligands library

Phytochemical components that comprise the chosen species were retrieved using the PubChem databases as well as identified using the Indian Medicinal Plants, Phytochemistry, And Therapeutics (IMPPAT) ingredient database [3]. 43 chemicals have been produced by the *M. sinesis & A. villosus*, and these substances were identified using the information databases listed in previously. The phytochemicals' smile identifiers were employed to conduct an inquiry on PubChem Server, as well as the outcomes were preserved in a file type called SDF.

3.8.2. Pharmacokinetics analysis

Pharmacokinetics (PK) is a xenobiotics control process that is necessary during preclinical research and medication development. It uses numerous mathematical calculations to provide a model to observe the ADME properties of foreign compounds (xenobiotics) in the body over time. The study of PK characteristics aids in the development and prediction of physiologically useful drug-like compounds. The drug-like properties of the 43 selected compounds for protein Alpha Glucosidase (PDB ID:3WY1) and Peroxisome proliferator-activated receptor gamma (PDB ID: 8B8Z) respectively, were analyzed in accordance with 'The Lipinski rule of Five' to generate a lead compound for antidiabetics activity. Using the Swiss ADME server, the PK characteristics of chosen compounds and the ADME properties such as Mol were analyzed. Refractivity, drug-likeness, surface area, and AMES toxicity were estimated and presented in Table 5. The PK properties of all the selected compounds were found to be efficient in this research study.

Additionally, predicting toxicity is a necessary phase in the current

Table 3
Statistical analysis of blood serum reduction compared with the control group.

	Control	Standard (Glibenclamide)	GRP. A (A. N) (500 mg/kg	GRP. B (A. N) 250 mg/kg	GRP. C (E. A) 500 mg/kg	GRP. D (A. EA) 250 mg/kg	GRP. E (A. E) 500 mg/kg	GRP. F (A. E) 250 mg/kg	GRP. G (M N) 500 mg/kg	GRP. H (M N) 250 mg/kg	GRP. I (M EA) 500 mg/kg	GRP. J (M EA) 250 mg/kg	GRP. K (M E) 500 mg/kg	GRP. L (M E) 250 mg/kg
Mean ± SD	2.04 ± 1.016	1.5168 ± 0.776	3.172 ± 2.703	1.28 ± 0.512	1.34 ± 0.343	0.99 ± 0.148	1.506 ± 0.69	1.116 ± 0.412	0.722 ± 0.0853	0.94 ± 0.219	1.009 ± 0.515	1.0504 ± 0.368	1.404 ± 0.697	1.413 ± 0.612
P-value		0.196986	0.200871	0.067441	0.072084	0.006168	0.180958	0.023867	0.000494	0.004424	0.015342	0.014088	0.134328	0.127623
Significance level		80.30 %	79.9 %	93.26 %	92.79 %	99.38 %	81.90 %	97.61 %	99.95 %	99.56 %	98.47 %	98.59 %	86.57 %	87.245

drug discovery process that helps in identifying the harmful effects of compounds on animals, humans, and plants. In silico toxicology is a branch of toxicity assessment that uses various methods to analyze compounds' toxicity (Raies & Bajic, 2016). Traditional drug discovery is a time-consuming and expensive method since it relies on a range of animal experiments to justify the compound's toxicity (Bharadwaj et al., 2021).In comparison to traditional drug discovery methods, computer-aided toxicity testing offers a quick and economical way of screening extremely toxic chemical compounds, reducing the number of biological experimental experiments. Therefore, numerous servers such as admetSAR 2.0, proTox-II, and pkcsm web server were used to determine the harmful effects of a total of six compounds and presented in Table 5.

3.8.3. *PASS online prediction for QSAR analysis*

All 43 phytocompounds were evaluated for their potential ability to hinder diabetes using PASS online tool (http://www.way2drug.com/passonline). The 6 phytocompounds were only chosen based on combined activities such as anti-diabetic, alpha-amylase, and alpha-glucosidase inhibitors. Higher Pa activities have medicinal efficacy as well as experiment production potential. In our QSAR model analysis of all the phytocompounds, we screened the best 6 phytocompounds by utilizing the Pa cut-off value $\geq$ 300 (greater or equal to 300) (Table 6). In addition, PASS can help to lessen a molecule's side effects even if it can't estimate the binding affinity for novel therapeutic targets. The selected 6 phytocompounds were taken for further analysis such as for site-specific super molecular docking after evaluating ADMET results.

3.8.4. *Quantum mechanics calculation*

In the DFT calculations of Alpha Glucosidase protein (PDB ID: 3WY1) protein, CID: 102506517, CID: 6327703, and CID: 441,314 (Control) generated LUMO and HOMO energy scores of −0.321414, −0.210409 and −0.053081 a.u. and −0.244952, −0.069404 and −0.490206 a.u. (Fig. 2 and Table 7). CID: 102506517, CID: 6,327,703 and CID: 441,314 (Control) generated HLG, hardness and softness score of 0.175548, 0.087774 and 11.39289539, 0.168792,0.084396 and 11.84890279, and 0.157328, 0.078664 and 12.71229533 a.u., respectively (Table 7). CID: 102,506,517 and CID:6327703 were chosen for further investigation and compared with CID: 441,314 (Control) compounds. In addition, Peroxisome proliferator-activated receptor gamma (PDB ID: 8B8Z), CID: 605775, CID: 605777, CID:15764573, CID: 91720824, and CID 77999 (Control) produced a HOMO and LUMO energy of −0.227911 and -0.008276, −0.227033 and −0.005782, −0.25189 and −0.048864, −0.25189 and −0.048354, −0.203625 and −0.034123 a.u respectively (Fig. 3 and Table 7). CID:605775, CID:6095777, CID:15764573, CID:91720824, and CID: 77,999 (Control) produced HLG, hardness and softness energy of 0.219635,0.1098175 and 9.106016801, 0.221251,0.1106255 and 9.039507166, 0.203026, 0.101513 and 9.85095505, 0.203536,0.101768 and 9.82627152, 0.169502,0.084751 and 11.79927081, respectively (Table 7).

3.8.5. *Site-Specific molecular docking and Post-Docking visualization*

Selected Phytocompounds from chosen species *M. sinesis* & *A. villosus* that interact with the Alpha Glucosidase (PDB ID: 3WY1) and Peroxisome proliferator-activated receptor gamma (PDB ID:8B8Z) proteins were found through molecular docking method using Maestro package platform. The Maestro program provided the best docking score between ligands and macromolecules. For Alpha Glucosidase (PDB ID: 3WY1) protein, the Control ligand Miglitol (CID: 441314) was used in this investigation, and it obtained −7.42 Kcal/mol binding affinity. The ligand, Phenyl isocyanide, 4,4′-methylenebis performed the best accurate score of −7.88 Kcal/mol, and the potential bioactive Phytocompounds, such as Diazo acetic acid (1S,2S,5R)-2-isopropyl-5-methylcyclohexyl ester exhibited the best docking value −7.73 Kcal/mol which are represented in Table 8. In addition, the control ligand Rosiglitazone (CID:77999) was used for Peroxisome proliferator-activated receptor gamma (PDB ID; 8B8Z) protein and obtained −9.43 Kcal/mol

Table 4
Statistical analysis of N-hexane, Ethyle acetate, and Ethanol extract of *Allophylus villosus* and *Mycetia sinensis,* respectively, for serum alkaline phosphatase.

	Control	Stan Dard (Glibenclamide)	GRP. A (A.N)	GRP. B (A.N)	GRP. C (A. EA)	GRP. D (A. EA)	GRP. E (A.E)	GRP. F (A.E)	GRP. G (M.N)	GRP. H (M.N)	GRP. I (M. EA)	GRP. J (M. EA)	GRP. K (M. E)	GRP. L (M. E)
			(500 mg /kg	250 mg/ kg	500 mg/ kg	250 mg/ kg	500 mg/ kg	250 mg/ kg	500 mg/ kg	250 mg/ kg	500 mg/ kg	250 mg/ kg	500 mg/ kg	250 mg/ kg
Mean ±SD	482. 096 ±152. 7567	393. 646 ±59. 2564	403. 586 ± 125. 14	278. 65 ± 152. 23	369. 602 ± 80.29	517. 1436 ± 119. 004	413. 533 ± 119. 004	530. 073 ± 110. 45	414. 2± 112. 85	426. 156 ± 181. 51	281. 3204 ± 131. 385	334. 52 24 ± 95. 76	291 0.50 48 ± 191. 76	335. 43 4± 139 0.810
P-value		0.12 48 41	0.2 02 70 1	0	0.0 80 15 5	0.33 80 15	0.25 87 17	0.2 82 93 3	0.2 28 52 2	0.3 13 45 6	0	0	0	0
Significance level		87. 5 %	79 0.7 %	100 %	91.9 8 %	66.2 0 %	74. 13 %	71. 71 %	77. 15 %	68. 65 %	100 %	100 %	100 %	100 %

Table 5
ADMET analysis and profiling of physiochemical and pharmacokinetics properties of selected for ligands for Alpha Glucosidase protein (PDB ID: 3WY1) and Peroxisome proliferator-activated receptor gamma (PDB ID: 8B8Z).

Ligands for Alpha Glucosidase protein (PDB ID: 3WY1)															
Compounds Details	**Physicochemical Properties**								**Pharmacological Properties**						
	MoW	**HAc**	**HD**	**NRB**	**MoR**	**SA**	**NLV**	**DL**	**IA**	**BBB**	**TC**	**AT**	**LD_{50}**	**HT**	**MTD**
CID:6327703 (Phenyl isocyanide, 4,4′-methylenebis)	220.27 g/mol	2	0	2	71.82	100.788	0	Yes	89.503	No	0.82	Yes	2.712	No	0.647
CID:102506517 (Diazo acetic acid (1S,2S,5R)-2-isopropyl-5-methylcyclohexyl ester)	224.30 g/mol	4	0	4	62.62	96.605	0	Yes	96.903	No	0.284	No	2.766	No	0.469
CID:441314 (Control) (Miglitol)	207.22 g/mol	6	5	3	51.08	82.019	0	Yes	41.462	No	0.815	No	2.257	No	2.239
Ligands for Peroxisome proliferator-activated receptor gamma (PDB ID: 8B8Z)															
CID: 605,775 (Pentanedioic acid, (2,4-di-t-butylphenyl) monoester)	320.42 g/mol	4	1	8	92.67	138.406	0	Yes	95.904	No	0.795	No	2.495	No	0.264
CID: 605,777 (2,4-Dit-butylphenyl 5-hydroxypentanoate)	306.44 g/mol	3	1	8	92.06	134.245	0	Yes	93.965	No	0.91	No	2.511	No	−0.192
CID:15764573 (Phthalic acid, di(oct-3-yl) ester)	390.56 g/mol	4	0	16	116.30	170.550	1	Yes	91.726	No	1.989	No	1.6	No	1.362
CID:91720824 (Phthalic acid, 6-methylhept-2-yl octyl ester)	390.56 g/mol	4	0	16	116.30	170.550	1	Yes	91.146	No	1.721	No	1.298	No	1.278
CID:77999 (Control)(Rosiglitazone)	357.43 g/mol	4	1	7	101.63	150.126	0	Yes	93.757	No	0.107	No	2.692	Yes	0.066

*ADMET: absorption, distribution, metabolism, excretion, and toxicity; IA: Intestinal absorption; HD: No. of hydrogen bond donor; HAc: No. of hydrogen bond acceptor; MW: molecular weight; TC: total clearance; NLV: No. of Lipinski's rule violations; DL: drug-likeness; MTD; maximum tolerated dose for a human, log mg mg/(kg.day); SA: surface area; AT: ames toxicity; MoR: Mol. Refractivity, BBB; blood brain barrier.

binding affinity. The ligand, Phthalic acid, 6-methylhept-2-yl octyl ester acquired the best binding score of −9.58 Kcal/mol, and the other potential bioactive Phytocompounds, such as Phthalic acid, di (oct-3-yl) ester, Pentanedioic acid, (2,4-di-t-butylphenyl) monoester and 2,4-Dit-butylphenyl 5-hydroxypentanoate displayed docking score of −9.25, −8.5, −8.48 Kcal/mol respectively and are shown in Table 8.

BIOVIA Discovery Studio Visualizer tool and Ligplot + version 2.2 was used to observe molecular interaction between selected ligands and targeted protein. All docked complexes were inputted into Ligplot + version 2.2, and the molecular interactions (Hydrogen and Hydrophobic bond) were calculated and shown in Figs. 4, 5, and Table 8.

3.8.6. Analysis of molecular dynamics simulation (MDS) trajectories

Molecular dynamics simulations (MDS) aid in the determination of the conformational strength of molecules and atoms by exhibiting the system at an atomistic scale. The MD simulation is an excellent and unique approach to determining the stability of a ligand in a targeted protein macromolecule. In this case, a 100 ns MD simulation was employed to examine the complex structure of the compounds that had been chosen. This was done to see how well the ligands could bind to the protein and the active site cavity of the protein. The results of MD simulation have been described based on RMSF, RMSD, MolSA, SASA, PSA, intramolecular hydrogen bonds (Intra HB), and protein–ligand contact analysis (P-L contact).

3.8.6.1. RMSD analysis. The root means square deviation (RMSD) of a protein–ligand complex system enables the determination of the average distance caused by a chosen atom's dislocation over a specified period. It is mostly the square root of the mean of squared errors that are used to figure out how much difference there is between two values (observed value and estimated value). The mean or average value changes from one frame to another with a range order of 1–5 Å or 0.1–0.5 nm is permissible, while a value outside the acceptable range indicates a significant conformational shift in the protein. The RMSD of the drug candidate Compound CID-102506517 (blue), CID-6327703 (orange), and the Control Drug (CID-441314) (ash) complex structure have been

Table 6
The QSAR result of selected phytocompounds and control ligands for bioactivity prediction for Peroxisome proliferator-activated receptor gamma (PDB ID: 8B8Z) protein and Alpha Glucosidase Protein (3WY1).

PubChem ID	Compounds Name	Pa	Pi	Activity
Ligands for Peroxisome proliferator-activated receptor gamma (PDB ID: 8B8Z)				
CID-91720824	Phthalic acid,6-methylhept-2-yl octyl ester	0,497	0,058	Glucan *endo*-1,3-beta-D-glucosidase inhibitor
		0,363	0,020	Glucan 1,4-beta-glucosidase inhibitor
		0,342	0,125	Diabetic neuropathy treatment
CID-15764573	Phthalic acid, di (oct-3-yl) ester	0,655	0,017	Glucan *endo*-1,3-beta-Glucan *endo*-1,3-beta-D-glucosidase inhibitor
		0,616	0,031	Glucan *endo*-1,6-beta-glucosidase inhibitor
		0,506	0,007	Glucan 1,4-beta-glucosidase inhibitor
		0,320	0,029	Prunasin beta-glucosidase inhibitor
CID-605777	2,4-Dit-butyl phenyl 5-hydroxy pentanoate	0,642	0,019	Glucan *endo*-1,3-beta-D-glucosidase inhibitor
		0,576	0,004	Glucan 1,4-beta-glucosidase inhibitor
		0,354	0,095	Glucan *endo*-1,6-beta-glucosidase inhibitor
		0,318	0,030	Antidiabetic symptomatic
		0,368	0,081	Diabetic neuropathy treatment
CID-605775	Pentanedioic acid, (2,4-di-t-butyl phenyl) monoester	0,323	0,026	Alpha-amylase inhibitor
CID-77999(Control)	Rosiglitazone	0,955	0,004	Antidiabetic
Ligands for Alpha Glucosidase (PDB ID: 3WY1)				
CID-102506517	Diazoacetic acid (1S,2S,5R)-2-isopropyl-5-methyl cyclohexyl ester	0,472	0,069	Glucan *endo*-1,3-beta-D-glucosidase inhibitor
CID-441314 (Control)	Miglitol	0,486	0,007	Alpha-amylase inhibitor
		0,375	0,007	Beta-amylase inhibitor
		0,330	0,009	Isoamylase inhibitor

compared with the protein human alpha-glucosidase (PDB ID: 3WY1) to observe the changes of the order, as shown in Fig. 6 **(A)**. The RMSD for two compounds was in a range between 1.2 Å and 3.7 Å with slight fluctuations that were perfectly acceptable compared to the structure of the native protein, and for the control drug, the fluctuation range was 1.2 Å to 6.0 Å. Similarly, in Fig. 6 **(B),** the RMSD of drug candidate Compound CID-605775 (blue), CID-605777 (orange), CID-15764573 (ash), CID-91720824 (yellow), and the Control Drug CID-77999 (light blue) with the protein activated transcription factor (PDB ID: 8B8Z) has been calculated. The average root means square deviation (RMSD) for the drug candidate Compound CID-605775 (blue), CID-605777 (orange), CID-15764573 (ash), CID-91720824 (yellow), and the Control Drug CID-77999 (light blue) was between 1.3 and 5.7 Å.

3.8.6.2. RMSF analysis. The RMSF is essential for monitoring local protein changes because it computes the average change detected across a large number of atoms and assesses the displacement of a specific atoms in comparison to the reference structure. This numerical calculation is similar to root mean square deviation and is significant for protein characterization because it may be used to evaluate the flexibility and fluctuation of the residues throughout the simulation (Rahman et al., 2022; Sarker et al., 2022). Consequently, the RMSF values of the experimental drug candidate Compound CID-102506517 (blue), CID-6327703(orange), and the Control Drug (CID-441314) (ash) in complex with human alpha-glucosidase (PDB ID: 3WY1) were calculated in order to analyze the alteration in protein structural flexibility caused by the attachment of the selected ligand compounds to a specific residual position, as illustrated in Fig. 6**(C)**. Additionally, the RMSF values of the selected drug candidate Compound CID-605775 (blue), CID-605777 (orange), CID-15764573 (ash), CID-91720824 (yellow), and the Control Drug CID-77999 (light blue) with the protein activated transcription factor (PDB ID: 8B8Z) are illustrated in Fig. 6**(D)**.

It was revealed that the most rigid secondary structural components, such as alpha-helices and beta-strands, have a minimum observation rate ranging from total amino acid residues of these targeted two proteins. Since the protein has both N- and C-terminal domains, most of the protein's variation may be found at these points. Consequently, it can be determined that the displacement of a single atom has a low fluctuation probability in the simulated environment for the ligand compounds under investigation, as shown in Fig. 6**(C) and (D)**.

3.8.6.3. The radius of gyration (Rg) analysis. A protein–ligand interaction complex's radius of gyration may be defined as the arrangement of its atoms around its axis. Rg calculation is one of the most essential indicators to look for when predicting a macromolecule's structural functioning since it exhibits changes in complex compactness over simulation time.

As a result, as shown in Fig. 7 **(A)**, the stability of the drug candidate Compound CID-102506517(blue), CID-6327703(orange), and the Control Drug (CID: 441314) (orange) in interaction with the target protein was studied in terms of Rg throughout a 100-ns simulation duration. The average Rg values for the drug candidate Compound CID-102506517 (blue), CID-6327703(orange), and the Control Drug (CID-441314) (ash) with the protein human alpha-glucosidase (PDB ID: 3WY1) were calculated at 2.5, and 3.9, suggesting that when the ligand was bound, the protein's binding site did not go through significant structural modifications.

In Fig. 7**(B)**, the stability of the drug candidate Compound CID-605775 (blue), CID-605777 (orange), CID-15764573 (ash), CID-91720824 (yellow), and the Control Drug CID-77999 (light blue) with selected protein activated transcription factor (PDB ID: 8B8Z) were calculated; the values were 3.7, and 6.1, showing that the protein's binding site does not undergo major structural change upon binding the selected ligand compounds.

Additionally, oxygen and nitrogen are the only atoms that contribute to the polar surface area (PSA) of a structure. Here, all the drug candidate Compound CID-102506517 (blue), CID-6327703(orange) and the Control Drug (CID-441314) (ash) with the targeted proteins human alpha-glucosidase (PDB ID: 3WY1) and the drug candidate Compound CID-605775 (blue), CID-605777 (orange), CID-15764573 (ash), CID-91720824 (yellow), and the Control Drug CID-77999 (light blue) with the targeted proteins activated transcription factor (PDB ID: 8B8Z) displayed a strong PSA value with the targeted protein (Fig. 8**C** and **D**), respectively.

3.8.6.4. Evaluation of intramolecular bonds. During 100 ns simulation period, the protein complexed with selected ligands and their intermolecular interactions have been explored using the "Simulation Interactions Diagram (SID)".These interactions (or 'contacts') of the drug candidate Compound CID-102506517 (blue), CID-6327703(orange), and the Control Drug (CID-441314) (ash) with the targeted proteins

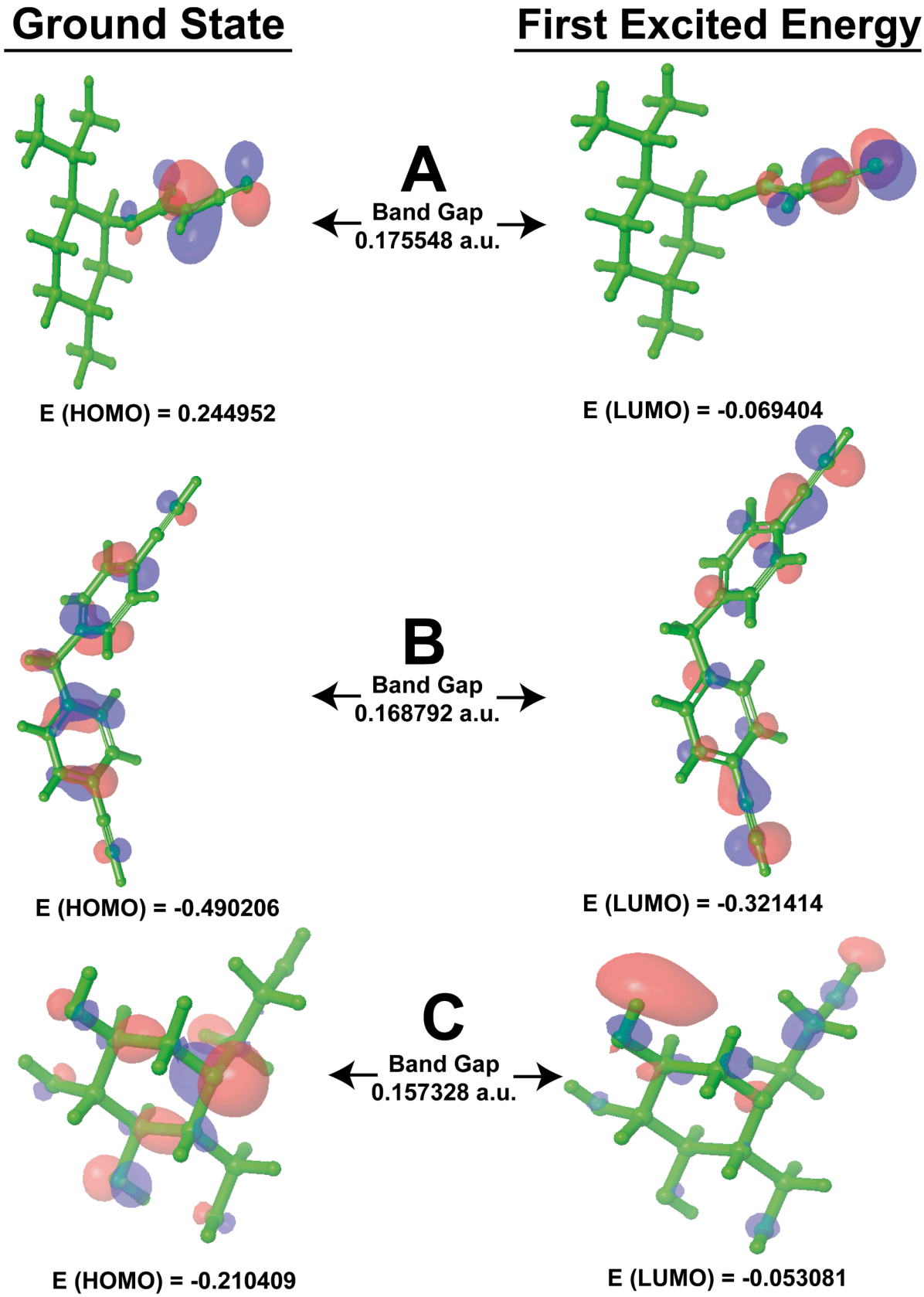

Fig. 2. The HOMO and LUMO energy score and structure of the 2 docked compounds were compared with control drug (C) for Alpha Glucosidase protein (PDB ID: 3WY1) protein.

Table 7
HOMO-LUMO, Softness and Hardness Studies of the selected two Compounds and control drug for Alpha Glucosidase protein (PDB ID: 3WY1) protein.

Ligands for Alpha Glucosidase (PDB ID: 3WY1)					
Molecules (chair)	**εHOMO**	**εLUMO**	**Gap**	**H (Hardness, Gap/2)**	**S (Softness, 1/Hardness)**
CID-102506517	−0.244952	−0.069404	0.175548	0.087774	11.39289539
CID-6327703	−0.490206	−0.321414	0.168792	0.084396	11.84890279
CID-441314 (Control)	−0.210409	−0.053081	0.157328	0.078664	12.71229533
Ligands for Peroxisome proliferator-activated receptor gamma (PDB ID: 8B8Z)					
CID-605775	−0.227911	−0.008276	0.219635	0.1098175	9.106016801
CID-605777	−0.227033	−0.005782	0.221251	0.1106255	9.039507166
CID-15764573	−0.25189	−0.048864	0.203026	0.101513	9.85095505
CID-91720824	−0.25189	−0.048354	0.203536	0.101768	9.82627152
CID-77999 (Control)	−0.203625	−0.034123	0.169502	0.084751	11.79927081

human alpha-glucosidase (PDB ID: 3WY1) and Compound CID-605775 (blue), CID-605777 (orange), CID-15764573 (ash), CID-91720824 (yellow), and the Control Drug CID-77999 (light blue) with the targeted proteins activated transcription factor (PDB ID: 8B8Z) have been described and displayed in Fig. 9 and Fig. 10. All compounds generated various intermolecular connections via hydrophobic, Water Bridge, hydrogen, and ionic bonds and maintained these connections until the simulations concluded, allowing the formation of a stable binding with the targeted protein.

3.8.7. Post MDS thermal MMGBSA calculation

For Alpha Glucosidase (PDB ID: 3WY1) MM-GBSA calculations of the chosen compounds CID: 102506517, CID:6327703 and CID: 441,314 (Control) generated negative MM-GBSA ΔG bind (NS) scores of −51.58, −80.43 and −57.84 Kcal/mol, respectively and for PRARG (PDB ID: 8B8Z) compound CID: 605775, CID:605777, CID:15764573, CID; 91,720,824 and the control drug (CID:77999) produced the negative MM-GBSA ΔG bind (NS) score of −97.86, −128.61, −107.71, −113.26 and −117.99 respectively. Furthermore, the analysis of binding free energy values for each docked complex of 3WY1-ligands and 8B8Z-ligands revealed the performance of ΔG Bind vdW (Van der Waal's interaction energy), ΔG Bind lipo (Lipophilicity energy), ΔG Bind Coulomb (Coulomb energy) in the complex stability. These results examined the strong binding of target compounds such as CID:6327703, CID: 102,506,517 in contrast to control drug (CID: 441314) of Alpha Glucosidase (Fig. 11**A**) and CID: 605775, CID: 605777, CID: 15764573, CID: 91720824, by comparison the control drug (CID: 77999) of (Fig. 11**B**).

4. Discussion

Rangamati Hill track area in Bangladesh is habitat of several indigenous people, of whom 49 % prefer self-made medicine to prescriptions from authorized doctors (Saha et al., 2022). As a potential alternative to pharmacological products, plant-derived compounds are increasingly gaining attention for their low side effects (Fatima et al., 2021). Indigenous medicine utilizes 80 % of associated medicinal plants (Fabricant & Farnsworth, 2001). *M. sinensis* and *A. villosus* are traditionally used to treat diabetes and hepatitis in the Chakma community. This study aims to investigate important phyto-chemicals such as alkaloids, flavonoids, phenols, carbohydrates etc., that could treat diabetes and related diseases (Bhat, 2021a).

A range of solvents with varying degrees of polarity, including n-hexane, ethyl acetate, and ethanol, were used in our study to extract compounds of unknown types (Altemimi et al., 2017; Doughari, 2012; Pandey & Tripathi, 2014). We obtained six extracts (three from each plant; *M. sinensis* and *A. villosus*) to determine flavonoid and phenol contents (Feudjio et al., 2020). According to other previous research, usually, ethanol extracts have a higher phenolic content than other solvent residues (Babbar et al., 2014; Nakamura et al., 2017) in *A.villosus*; as new findings, we have noticed that the phenolic content of ethyl acetate extract of *M. Sinensis* surpassed rest of the two extracts. Additionally, n-hexane fractions surpassed ethyl acetate fractions in *M. sinensis* and *A. villosus* for flavonoid contents. Both, Phenolic and flavonoid compounds are capable in glucose homeostasis mechanism (Al-Ishaq et al., 2019; Deka et al., 2022) as well as performed inhibitory activities on alpha glucosidase and PPAR-γ (Proença et al., 2017; Salam et al., 2008; Swargiary et al., 2023).

Table S1**a-f,** presents the FTIR analysis results of the extracts, It were observed that the N-hexane extract of *M. sinensis* corresponding to phenol's O—H bending, aromatic compounds' C—H bending, esters and aldehydes' C═O stretching, carbon dioxide's O═C═O stretching, carboxylic acids' O—H stretching, aldehyde and alkane stretching, amine salt stretching, and carboxylic acid and alcohol stretching. A variety of functional groups were found in the peaks of ethyl acetate and ethanol extracts, including phenols, alcohols, amines, aromatic compounds, δ-lactones, primary and secondary amines, amine salts, alkyl aryl ethers, esters, carboxylic acids, and nitro compounds. Moreover, the extracts of *A. villosus* in hexane, ethyl acetate, and ethanol represent different phytochemical groups / functional groups, including carboxylic acids, amines, amides, sulfur derivatives, polysaccharides, organic hydrocarbons, and halogens, play a significant role in their medicinal properties (Maobe et al., 2021). These phytochemicals have been reported to have a high efficacy in hypoglycemic and hepatic function, making them potential therapeutic agents for the treatment of diabetes (Lu et al., 2010).

In previous investigations of GC we have found number of peaks for ethyl acetate and ethanol extract where n- hexane fractioned extracts for both plants haven't performed any significant peaks. Considering the previous analysis of GC we have decided to skip n- hexane fractioned extracts for further investigation on GC–MS. GC analysis of n- hexane fractioned extract for *Allophylus villosus* and *Mycetia sinensis* have shown in **figure S3** which reported only the solvent, on the other hand, GC report of ethyl acetate and ethanol fractioned extract leads us to further investigation on GC–MS. *Allophylus villosus* chromatogram has plotted in **figure S3 (a)** where **figure S3 (b)** represent the peak of *Mycetia sinensis*, both of the plants performed only solvents of n-hexane and ethanol. As the better investigation, GC–MS chromatographic analysis was conducted to identify phytochemicals with the potential to treat diabetes (Dada-Adegbola et al., 2022; Tittikpina et al., 2022). Therefore, we conducted GC–MS analysis to identify the phytochemicals, along with their molecular masses, molecular formulas, and chemical identities, from ethyl acetate and ethanol extracts of *M. sinensis*, and *A. villosus*. A total of 24 chemicals were identified in *M. sinensis* extracts, whereas 19 were identified in *A. villosus* extracts. In both ethyl acetate and ethanol extracts of *M. sinensis*, diazo acetic acid, 2-isopropyl-5-methylcyclohexyl ester, tetraethyl silicate, and phthalic acid, 6-methylhept-2-yl octyl ester, were commonly found. Both ethyl acetate and ethanol extracts of *A. villosus* contained diethyl-borinic acid, trichloromethane, tetraethyl silicate, pentanoic acid, 5-hydroxy-, and 2,4-di-t-butylphenyl esters. As these phytochemicals are identified, they can be explored further for their therapeutic properties as well as their potential to be developed

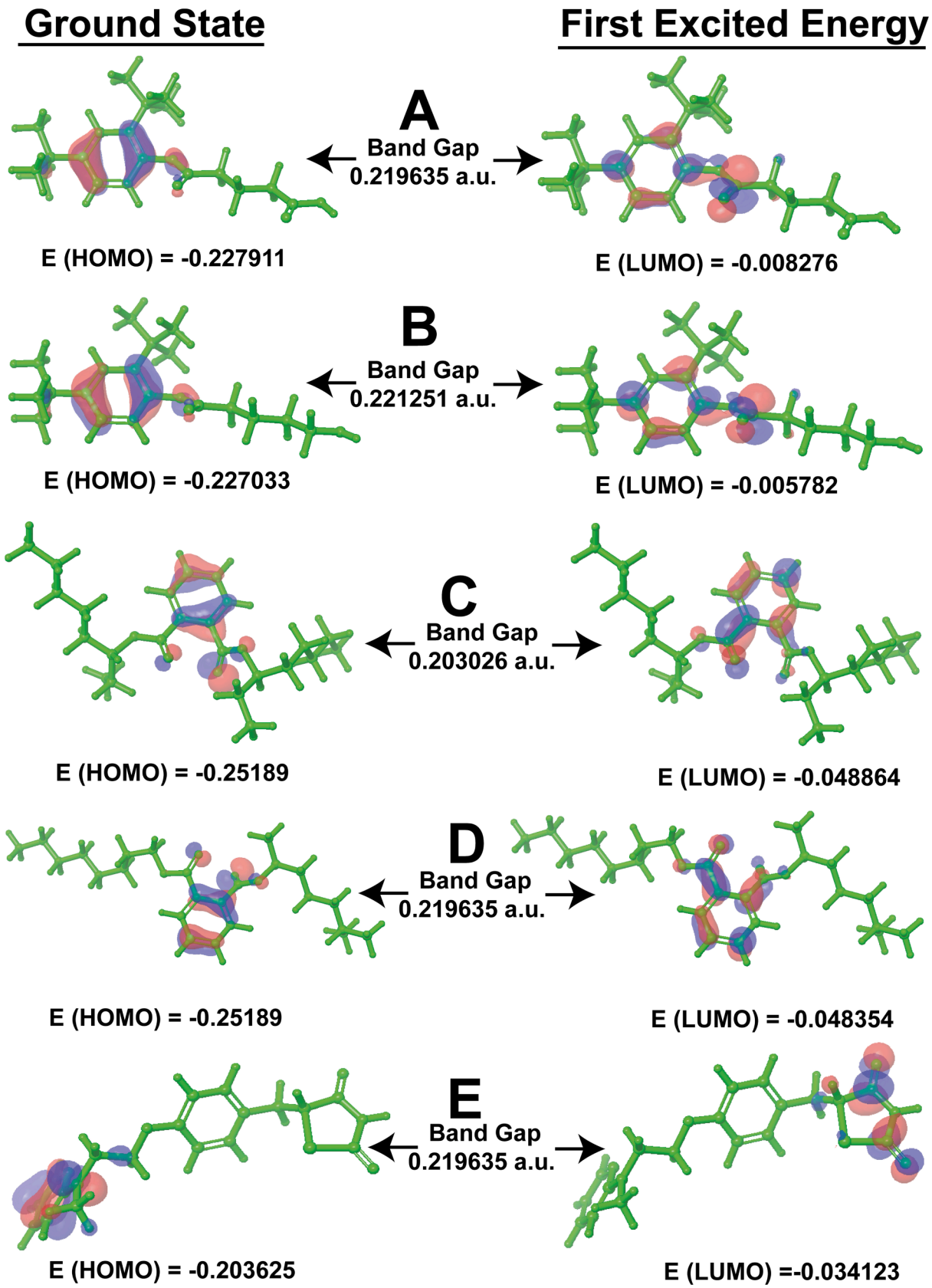

Fig. 3. The HOMO and LUMO energy score and structure of the 4 docked compounds were compared with control drug (E) for Peroxisome proliferator-activated receptor gamma (PDB ID: 8B8Z).

Table 8
The binding affinity between macromolecule Alpha Glucosidase (PDB ID: 3WY1) and selected phytocompounds and control drug. The intermolecular interaction between them and their binding affinity.

Ligands for Alpha Glucosidase (PDB ID:3WY1)				
Ligands PubChem CID Number	**Compounds Name**	**Docking Score (Kcal/mol)**	**Amino Acid Involved Interaction**	
			Hydrogen Bond Interaction	**Hydrophobic Bond Interaction**
CID: 6,327,703	Phenyl isocyanide, 4,4′-methylenebis	−7.88		Val102, Tyr65, Asp202, Asp333, Arg400, Gly228, Phe297, Glu271, Phe166, Thr203, His105
CID:102506517	Diazo acetic acid (1S,2S,5R)-2-isopropyl-5-methylcyclohexyl ester	−7.73	Glu271-2.96 Å, Arg200-2.97 Å	Arg400, Asp333, Phe166, His105, Asp202, Thr203, Gly273, Phe206
CID:441314 (Control)	Miglitol	−7.42	Arg200-2.99 Å, Arg200-2.83 Å, Arg400-3.16 Å, Gly228-2.94 Å, Gly228-3.21 Å, Asp202-2.63 Å	Asp333, His332, Tyr389, Ile146, Glu271, Gly273, Thr203, Tyr65
Ligands for Peroxisome proliferator-activated receptor gamma (PDB ID: 8B8Z)				
CID: 91,720,824	Phthalic acid, 6-methylhept-2-yl octyl ester	−9.58	Ser342-3.23 Å, Ser342-3.14 Å	His266, Gly284, Phe287, Phe264, Arg288, Leu330, Ile326, Met329, Ala292, Ile341, Ile281, Ala285
CID: 15,764,573	Phthalic acid, di(oct-3-yl) ester	−9.25	Ser342-2.94 Å	Gly284, Phe264, Ile281, Ile341, Met364, Leu353, Val339, Ile326, Arg288, Ser289, Ala285, Lys265, His266
CID: 605,775	Pentanedioic acid, (2,4-di-t-butylphenyl0 mono-ester	−8.5	His266-2.86 Å, Lys265-2.72 Å	Ser342, Phe287, Gly284, Ala285, Phe363, Met364, Ile281, Leu353, Arg288, Ile341, Val339, Leu340, Leu330, Phe264
CID:605777	2,4-Dit-butylphenyl 5-hydroxypentanoate	−8.48	Arg280-2.68 Å	Phe264, Gly284, Arg288, Leu330, Val339, Leu333, Leu340, Met364, Ala285, Phe363, Ile341, Ile281
CID:77999 (Control)	Rosiglitazone	−7.42	Lys265-2.97 Å, Ser342-2.98 Å	Val339, Phe363, Met364, Ala285, Ile281, Gly284, Phe264, Arg288, Ser289, Ile341, Leu330

into new drugs (Proestos & Komaitis, 2013; Proestos et al., 2006). Furthermore, both plant extracts were evaluated for their bioactivity regarding oral glucose tolerance, serum creatinine, and serum alkaline phosphatase.

Following the protocol of Bari et al., 2020 (Bari et al., 2020), 14 groups of Swiss albino mice were tested for oral glucose tolerance. As part of this study, every group was given extracts of *M. sinensis* and *A. villosus*, including n-hexane, ethyl acetate, and ethanol extracts of various doses from comparison with control. There was a significant difference between the experimental and control groups regarding blood glucose levels, indicating the extracts were effective (Benedé-Ubieto et al., 2020) as well as the glucose inhibition percentages were remarkable (**Figure S4**). Significant reductions were observed in groups receiving 250 mg/kg doses of all extracts after 30 min, whereas groups receiving 500 mg/kg doses showed significant reductions after 60 min. Compared to the 250 mg/kg dose and the initial value, the 500 mg/kg dose showed a more pronounced antihyperglycemic effect. Both plant extracts were shown to be significantly anti-hyperglycemic overall. Amino acids, polysaccharides, flavonoids, phenolic, alkaloids, coumarins, inorganic ions, and guanidine's, among other secondary metabolites, have been found to be anti-hyperglycemic by (Zilani et al., 2018). In the tested extracts, phenols, flavonoids, and other phytochemicals may improve glucose homeostasis and B-cell function (Fenercioglu et al., 2010).

As the diabetes complications for Kidneys and liver, in this study, blood serum creatinine levels were examined for the 14 groups, and results were significant ($p <= 0.05$) for all groups except Group A, Group E, Group K, and Group L. The creatinine test does not show a significant effect of Glibenclamide (Erejuwa et al., 2010). The standard group also showed insignificant results in this study compared to the control group, suggesting that anti-hyperglycemic actions may sometimes be accompanied by side effects (Erejuwa et al., 2010). Despite this, *A. villosus* and *M. sinensis* extracts performed well among the 12 treatment groups, and the results suggest that these extracts do not adversely affect kidney function. In addition, serum alkaline phosphatase levels were assessed in 12 different treatment groups using *M. sinensis* and *A. villosus* extracts. Significant results were observed in Groups B, I, J, K, and L. The I and J groups were administered 500 mg and 250 mg of ethyl acetate extracts of *M. sinensis*, respectively, while the K and L groups received 500 mg and 250 mg of ethanol extracts, respectively. Previously, n-hexane-derived extracts from *A. villosus* have been found to have significant hepatoprotective effects (Gazor et al., 2017). This study explored the phytochemical composition, anti-hyperglycemic activity, and effects of *A. villosus* and extracts on the kidney and liver. Besides exhibiting significant anti-hyperglycemic effects, the extracts also showed normal serum creatinine levels, indicating that they did not adversely affect renal function. The extracts also significantly reduced serum alkaline phosphatase levels, indicating hepatoprotective effects. The observed bioactivities may be mediated by various phytochemicals, including flavonoids and phenolic compounds. Therefore, *A. villosus* and *M. sinensis* can be used to develop antidiabetic agents with favorable safety profiles. The active compounds are responsible for these beneficial effects have been investigated in further research through *in-silico* approaches.

In recent times, in silico drug design plays an important role in the drug development process. It reduces the cost of identifying potential drug candidates by lowering the usage of animal models in pharmaceutical experiments by analyzing multiple techniques. These techniques include homology, visualization, molecular docking, and molecular dynamics study (Brogi et al., 2020; Wadood et al., 2013). High-quality drug candidates can be produced by analyzing the data obtained from multiple techniques used in silico drug development. However the current drug development process is highly costly and generally faces many unwanted failures in various stages. The scarcity of safety and effectiveness is the main reason for failure, which is usually associated with absorption, distribution, metabolism, excretion, and toxicity properties. For this purpose, ADMET profiling is used for rapid ADMET test of the selected compounds to reduce the failure of the drug

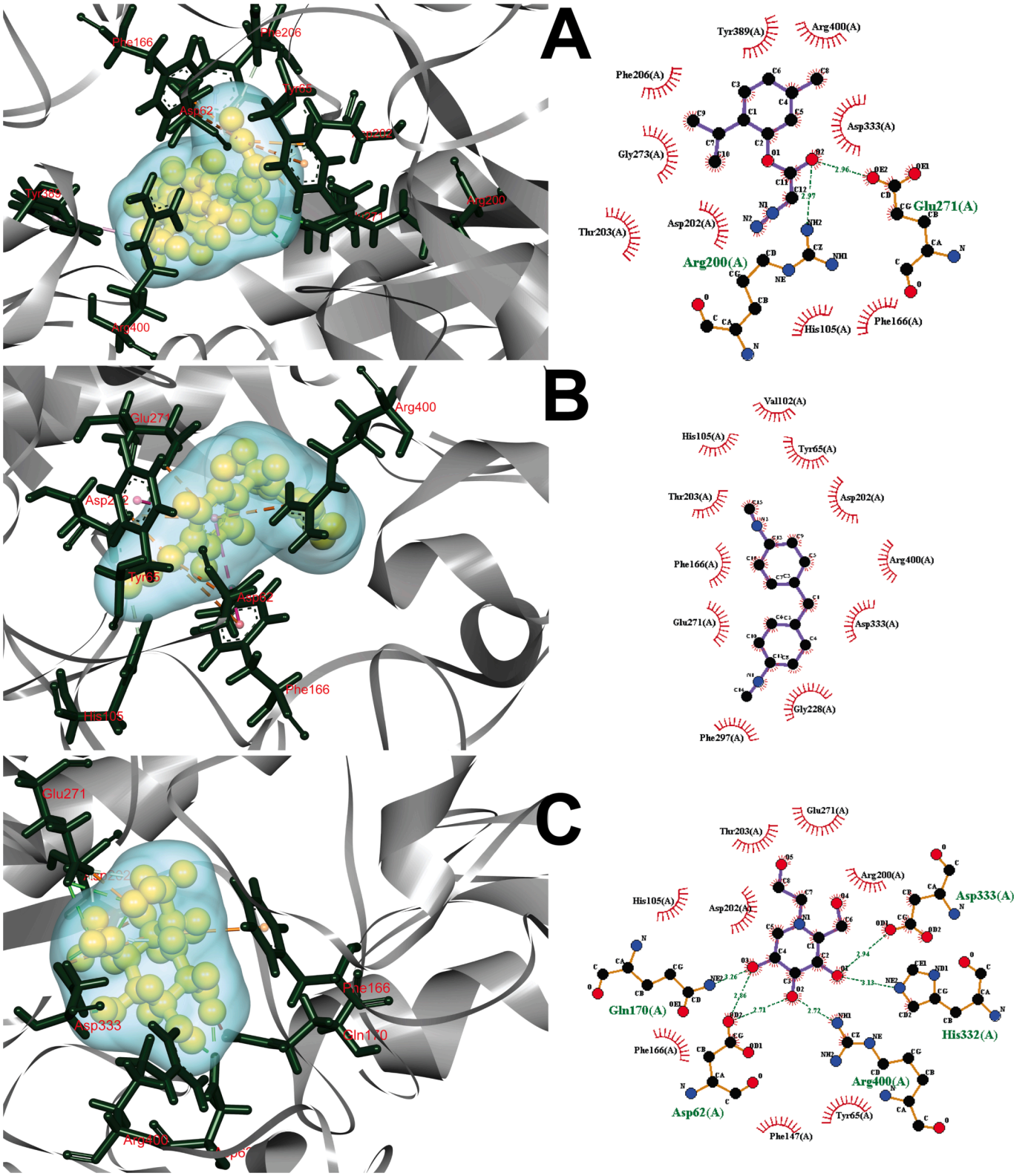

Fig. 4. Post docking Protein-Ligand interaction between Alpha Glucosidase (PDB ID: 3WY1) and selected phytocompounds and control ligands. On the left 3D figures and on the right 2D figures remain. **A**) 3WY1-CID:102506517**B**) 3WY1-CID:6327703**C**) 3WY1-CID:441314 (Control Drug).

development process (Biswas et al., 2022a; Dong et al., 2018; Hasan et al., 2022a; Hasan et al., 2022b). Forty-three compounds were obtained from *M. sinensis* & *A. villosus,* of which eight compounds, including six selected compounds and two control, the ADMET properties are computed by web-based servers such as SwissADME and pkCSM detailed in Table 5.

Quantum Mechanics has been utilized for further assessment of small molecules. In this case, HOMO and LUMO aid in understanding kinetic stability and chemical reactivity. HOMO-LUMO gap energy calculations were done in order to measure molecular forcefulness. All the substances

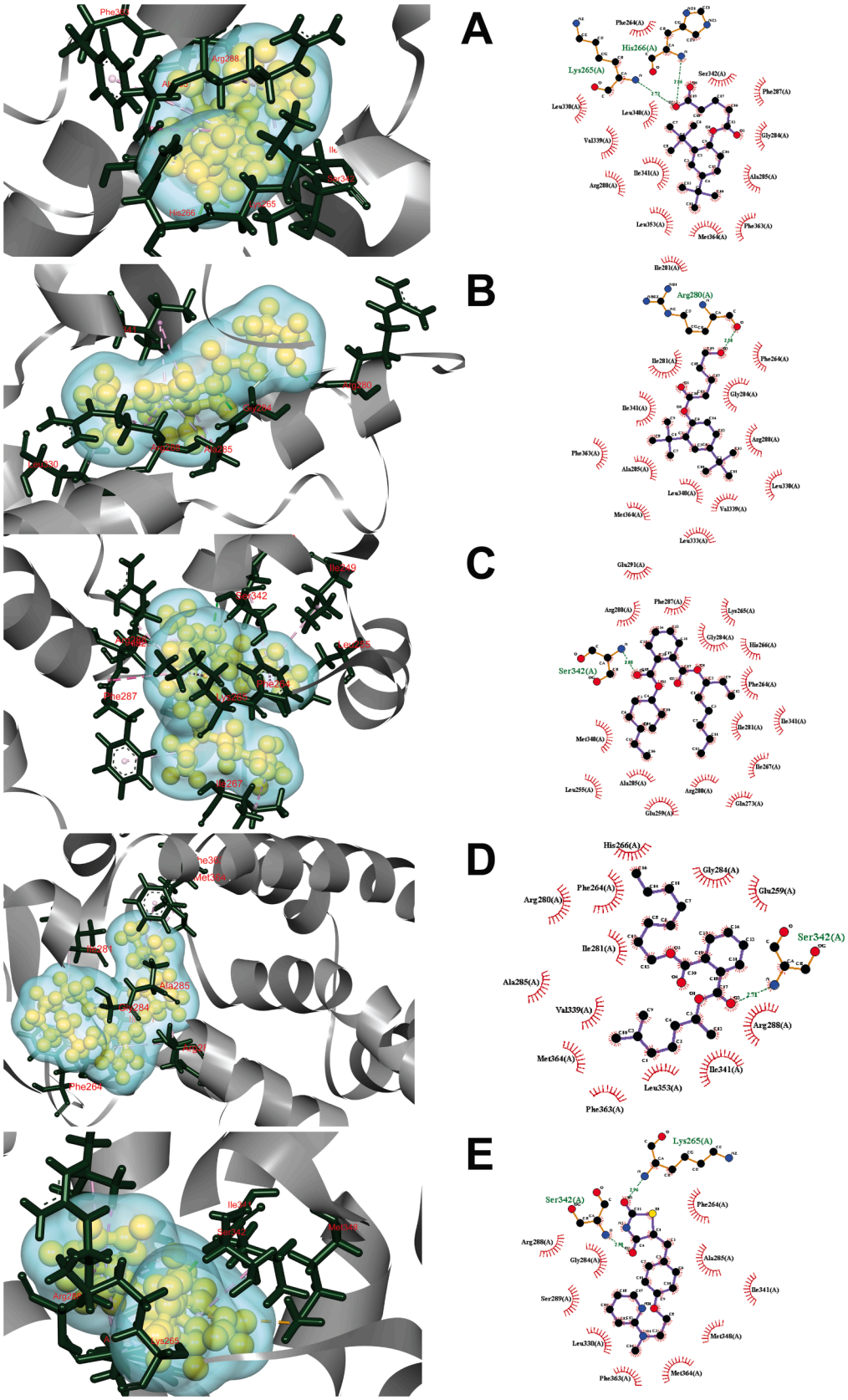

Fig. 5. Post docking Protein-Ligand interaction between Peroxisome proliferator-activated gamma (PDB ID: 8B8Z). On the left 3D figures and on the right 2D figures remain. **A**) 8B8Z- CID:605775**B**) 8B8Z-CID:605777**C**) 8B8Z-CID: 15,764,573 **D**) 8B8Z-CID:91720824 **E**) 8B8Z-CID:77999 (Control Drug).

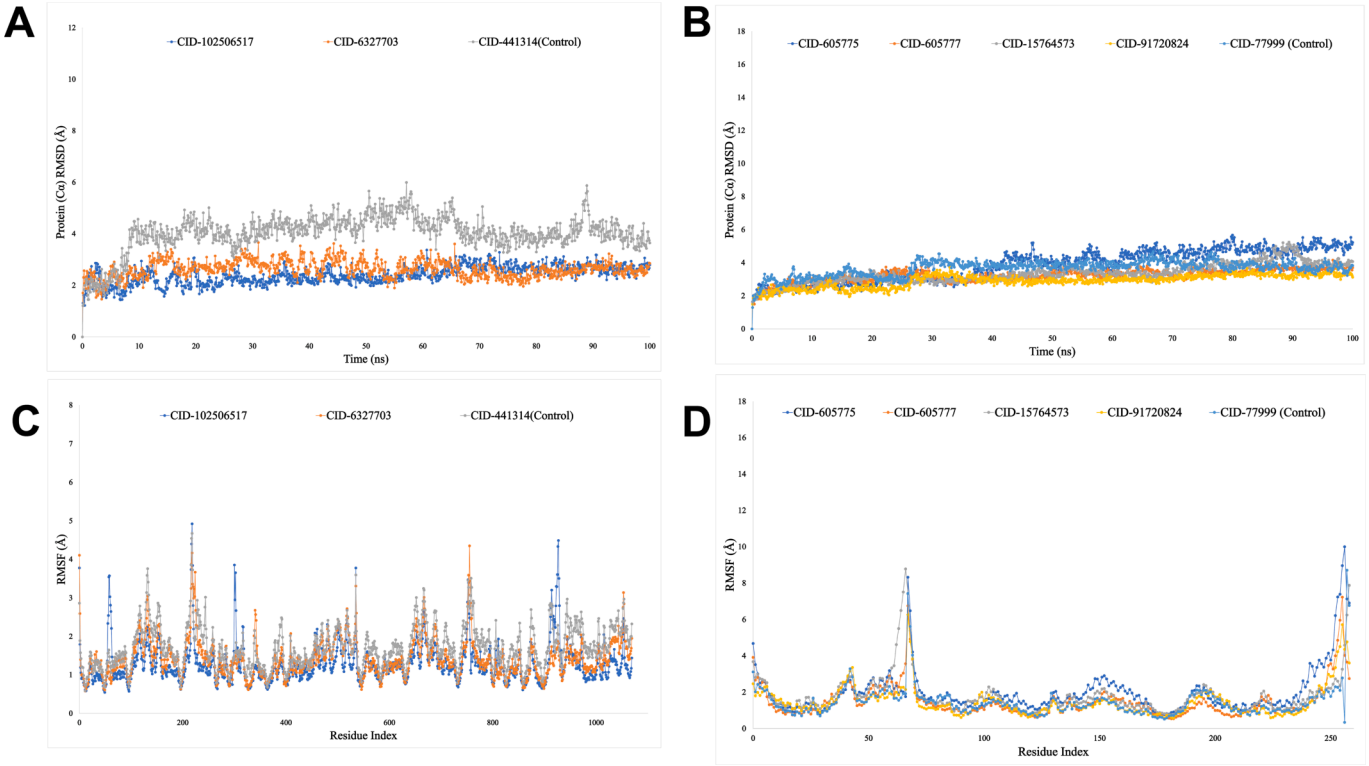

Fig. 6. (**A**) The graphs show the RMSD values for the three ligand molecules in complex with the targeted protein human alpha-glucosidase (PDB ID: 3WY1) in 100 ns MDS assessments, where the selected three ligands, the candidate Compound CID-102506517, CID-6327703 and the Control Drug (CID-441314) is associated with the protein are exhibited by blue, orange and ash color. and (**B**) The graphs show the RMSD values for the five ligand molecules in complex with the targeted protein-activated transcription factor (PDB ID: 8B8Z) in 100 ns MDS assessments, where the selected five ligands, the Compound CID-605775, CID-605777, CID-15764573, CID-91720824, and the Control Drug (CID-77999) is associated with the protein are exhibited by blue, orange, ash, yellow and light blue color (**C**) The RMSF values for the three ligand molecules in complex with the targeted protein human alpha-glucosidase (PDB ID: 3WY1) in 100 ns MDS assessments, where the selected three ligands, the candidate Compound CID-102506517, CID-6327703 and the Control Drug (CID-441314) is associated with the protein are exhibited by blue, orange and ash color. (**D**) The RMSF values for the five ligand molecules in complex with the targeted protein-activated transcription factor (PDB ID: 8B8Z) in 100 ns MDS assessments, where the selected five ligands, the Compound CID-605775, CID-605777, CID-15764573, CID-91720824, and the Control Drug (CID-77999) is associated with the protein are exhibited by blue, orange, ash, yellow and light blue color. (For interpretation of the references to color in this figure legend, the reader is referred to the web version of this article.)

have more significant than 0.15 gap energy, indicating dynamically opposed to undertake a chemical reaction, and are called bioactive components. Molecular docking is used to anticipate the binding configuration of the ligands centrally located to the protein and the association between protein and ligands. Maestro program was used to determine binding affinity of the selected phytocompounds through using site-specific super molecular docking to calculate binding score (David et al., 2018). For a target Alpha Glucosidase (PDB ID:3WY1), 43 compounds from *M. sinensis* & *A. villosus* and control drug Miglitol (CID-441314) was selected, the control drug acquired −7.42 Kcal/mol. Selected phytocompounds such as Phenyl isocyanide, 4,4′-methylenebis (CID-6327703) and Diazo acetic acid (1S,2S,5R)-2-isopropyl-5-methyl-cyclohexyl ester displayed −7.88 and −7.73 Kcal/mol respectively represented in Table 8. For Peroxisome proliferator-activated receptor gamma protein (PDB ID: 8B8Z), control drug Rosiglitazone and 43 phytocompounds are used for molecular docking. The control drug Rosiglitazone shows −9.43 Kcal/mol binding affinity and the four selected phytocompounds such Phthalic acid, 6-methylhept-2-yl octyl ester 9CID: 91720824), Phthalic acid, di(oct-3-yl) ester (CID: 15764573), Pentanedioic acid, (2,4-di-t-butylphenyl) mono-ester (CID: 605775) and 2,4-Dit-butylphenyl 5-hydroxypentaneoate (CID: 605777) displayed the binding affinity −9.58, −9.25, −8.5 and 8.48 Kcal/mol respectively and was shown in Table 8. In the next step, Ligplot + (version 2.2) was used to visualize 2D protein–ligand interaction and additional tools such as Biovia Discovery Studio were also used for 3D protein–ligand visualization.

When a protein is in a complex with ligands, molecular dynamic modeling can be used to ensure the compactness of the protein-ligands complexes. Additionally, it is capable of determining the stability of protein–ligand complexes in a given environment, such as the human body. There is a way to figure out how stable the compound is by looking at the RMSD value. The RSMF value is also used to figure out how much the protein–ligand complex changes over time. In this investigation, we used the Schrödinger package software (Desmond Application) to run a 100-ns Molecular Dynamic Simulation (MDS) with the physiological and physicochemical parameters of interest (Abdullah et al., 2023; Ahmed et al., 2023; Andalib et al., 2023; Sohel et al., 2022). There have been different ways to look at this simulation trajectory of the simulation tool. It has been used to look at things like the root mean square deviation (RMSD) and root mean square fluctuation (RMSF). The radius of gyration (Rg), hydrogen bond number, solvent accessible surface area (SASA), MolSA, and PSA have also been looked at. In complex systems, the lowest root means square deviation (RMSD) values suggest the best stability of the compounds, whereas the higher root means square fluctuation (RMSF) values indicate the lower compactness of the protein–ligand complex (Al Saber et al., 2022; Biswas et al., 2023a; Biswas et al., 2023b). The drug candidate Compound CID-102506517 (blue) showed the potent RMSD and RMSF values with the targeted proteins human alpha-glucosidase (PDB ID: 3WY1) compared to the Control Drug (CID-441314) (ash). On the other hand, CID-605777 (orange) showed potent RMSD and RMSF values with the targeted proteins activated transcription factor (PDB ID: 8B8Z) compared to the Control Drug CID-

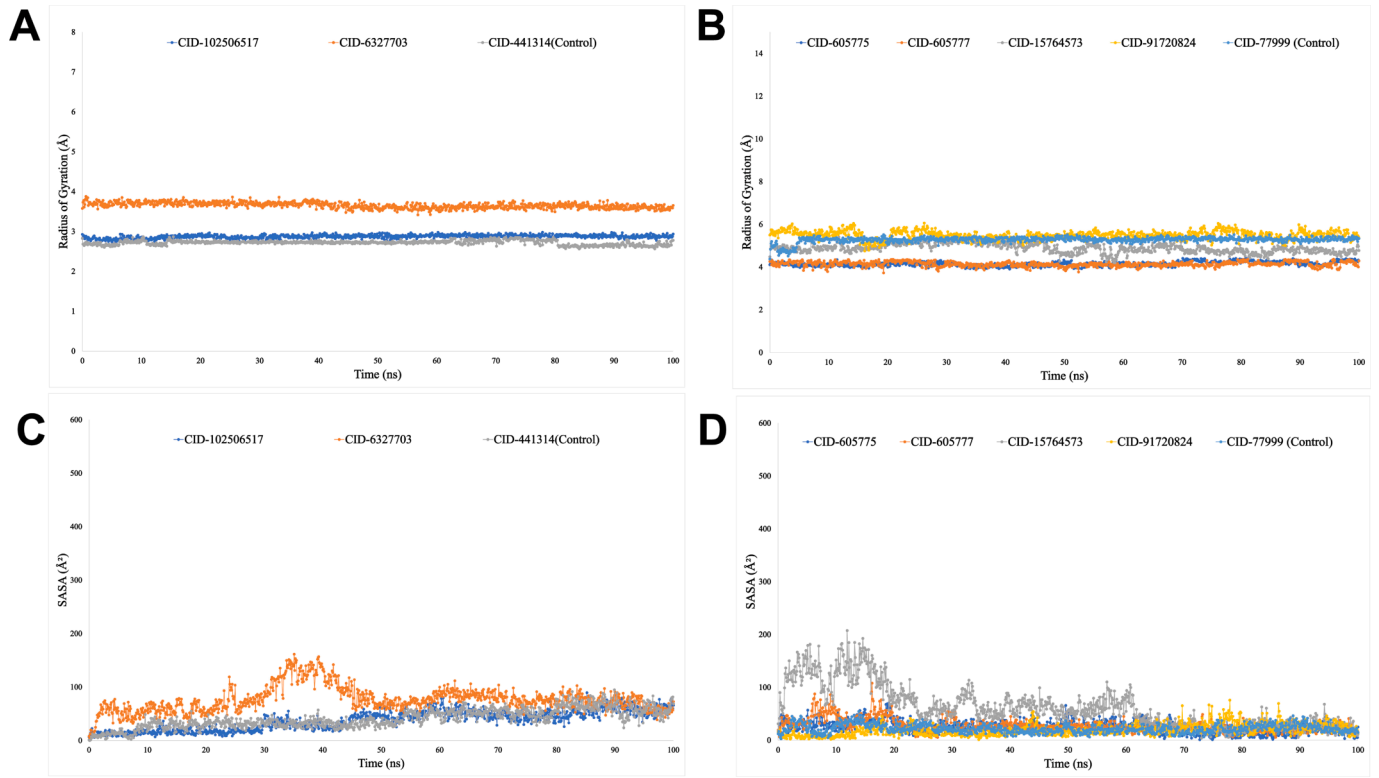

Fig. 7. (**A**) The graphs show the radius of gyration (Rg) values for the three ligand molecules in complex with the targeted protein human alpha-glucosidase (PDB ID: 3WY1 in 100 ns MDS assessments, where the selected three ligands, the Compound CID-102506517, CID-6327703 and the Control Drug (CID-441314) is associated with the protein are exhibited by blue, orange and ash colour (**B**) The graphs show the radius of gyration (Rg) values for the five ligand molecules in complex with the targeted protein-activated transcription factor (PDB ID: 8B8Z) in 100 ns MDS assessments, where the selected five ligands, the Compound CID-605775, CID-605777, CID-15764573, CID-91720824, and the Control Drug CID-77999 is associated with the protein are exhibited by blue, orange, ash, yellow and light blue colour. (**C**) The graphs show the SASA values for the three ligand molecules in complex with the targeted protein human alpha-glucosidase (PDB ID: 3WY1) in 100 ns MDS assessments, where the selected three ligands, the Compound CID-102506517, CID-6327703 and the Control Drug (CID-441314) is associated with the protein are exhibited by blue, orange and ash colour and (**D**) The graphs show the SASA values for the five ligand molecules in complex with the targeted protein-activated transcription factor (PDB ID: 8B8Z) in 100 ns MDS assessments, where the selected five ligands, the Compound CID-605775, CID-605777, CID-15764573, CID-91720824, and the Control Drug CID-77999 is associated with the protein are exhibited by blue, orange, ash, yellow and light blue colour. (For interpretation of the references to color in this figure legend, the reader is referred to the web version of this article.)

77999 (light blue) (Fig. 6).

The stability of the protein structure is tested by measuring the center of mass from its C and N terminals, and this data helps researchers better understand how proteins fold when Rg is determined (Jabin et al., 2023; Khan et al., 2023; Khan et al., 2021). With both the targeted proteins human alpha-glucosidase (PDB ID: 3WY1) and activated transcription factor (PDB ID: 8B8Z), the lower Rg value indicates great compactness, while the higher value indicates disassociation of the compounds from the protein. In our research study, the drug candidate Compound CID-102506517 (blue) had a standard Rg value compared to the Control Drug (CID-441314) (ash) with the targeted proteins human alpha-glucosidase (PDB ID: 3WY1). And for activated transcription factor (PDB ID: 8B8Z), both drug candidates Compound CID-605775 (blue) and CID-605777 (orange) had a lower Rg value compared to the Control Drug CID-77999 (light blue) (Fig. 7**A** and Fig. 7**B**). In addition, the simulation trajectories were used to figure out how the drug-like molecules changed in size over time. The solvent-accessible surface area (SASA) of the protein-ligands complex was also calculated. The higher the SASA value, the less stable structure, and the lower the SASA value, the more tightly packed the water molecules and amino acid residues are in the protein-ligands complex (Biswas, Hany Rumi, et al., 2022). According to the SASA result from the MDS trajectory, the drug candidate Compound CID-102506517 (blue) exhibited lower SASA values with proteins human alpha-glucosidase (PDB ID: 3WY1) compared to the Control Drug (CID-441314) (ash) (Fig. 7**C**), whereas in case of activated transcription factor (PDB ID: 8B8Z), both drug candidate Compound CID-605777 (orange), and the Control Drug CID-77999 (light blue) presented almost the same SASA value and sometimes Compounds-605777 (orange) show lower SASA value (Fig. 7**D**). In the graph of PSA and MolSA validation, both drug candidates, Compound CID-102506517 (blue) and CID-6327703 (orange), possessed a potential value than the Control Drug (CID-441314) (ash) with the targeted proteins human alpha-glucosidase (PDB ID: 3WY1) (Fig. 8**A** and Fig. 8**B**). Moreover, in the graph of PSA and MolSA validation, both drug candidates Compound CID-605775 (blue), CID-605777 (orange), CID-15764573 (ash), CID-91720824 (yellow) possessed the potential value than the Control Drug (CID-77999 (light blue) with the targeted proteins human activated transcription factor (PDB ID: 8B8Z) (Fig. 8**C** and Fig. 8**D**) Furthermore, the "Simulation Interaction Diagram (SID)" was used to explore intermolecular interactions between proteins in complex with specified ligands over the length of 100 ns simulation. During the simulation, all ligands formed various intermolecular interactions by hydrophobic, water bridge, hydrogen, and ionic bond and maintained these interactions until the simulation was completed, facilitating the formation of formation of a stable binding with the targeted two proteins (Figs. 9 and 10). After MDS (Molecular Dynamics Simulation), we calculated binding free energy (thermal MM-GBSA) of all the compounds with the target receptor and all compounds possessed potent binding free energy compared to the control drug (Fig. 11).

Our research findings asserted that 2,4-Dit-butylphenyl 5-hydroxypentanoate and Diazo acetic acid (1S,2S,5R)-2-isopropyl-5-methylcyclohexyl ester obtained from *M. sinensis* & *A. villosus* through GC–MS

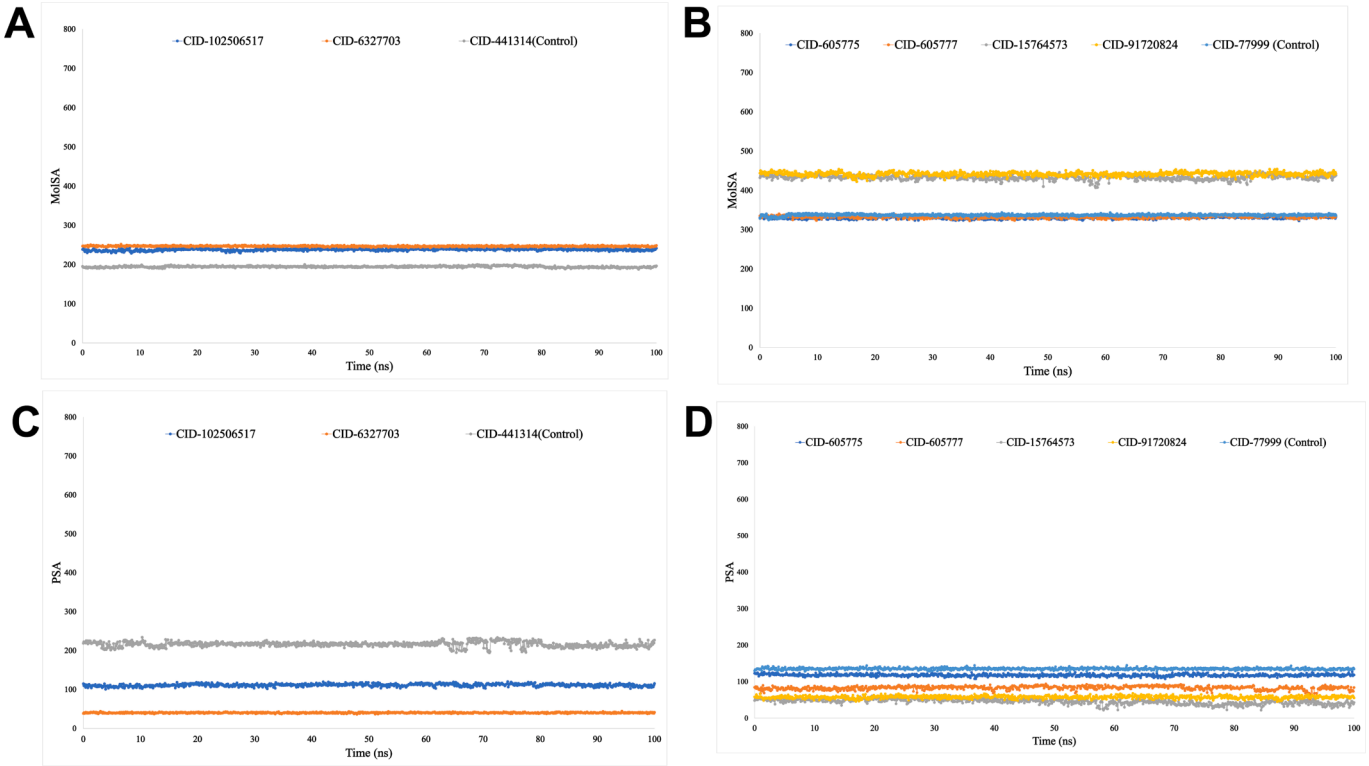

Fig. 8. (**A**) The graphs show the MolSA values for the three ligand molecules in complex with the targeted protein human alpha-glucosidase (PDB ID: 3WY1) in 100 ns MDS assessments, where the selected three ligands, the Compound CID-102506517, CID-6327703 and the Control Drug (CID-441314) in associated with the protein are exhibited by blue, orange and ash color (**B**) The graphs show the MolSA values for the five ligand molecules in complex with the targeted protein activated transcription factor (PDB ID: 8B8Z) in 100 ns MDS assessments, where the selected five ligands, the Compound CID-605775, CID-605777, CID-15764573, CID-91720824, and the Control Drug CID-77999 in associated with the protein are exhibited by blue, orange, ash, yellow, light blue color. (**C**) The graphs show the PSA values for the three ligand molecules in complex with the targeted protein human alpha-glucosidase (PDB ID: 3WY1) in 100 ns MDS assessments, where the selected three ligands, the Compound CID-102506517, CID-6327703 and the Control Drug (CID-441314) in associated with the protein are exhibited by blue, orange and color. (**D**) The graphs show the PSA values for the five ligand molecules in complex with the targeted protein activated transcription factor (PDB ID: 8B8Z) in 100 ns MDS assessments, where the selected five ligands, the Compound CID-605775, CID-605777, CID-15764573, CID-91720824, and the Control Drug CID-77999 in associated with the protein are exhibited by blue, orange, ash, yellow, light blue color. (For interpretation of the references to color in this figure legend, the reader is referred to the web version of this article.)

have medicinal effects against Alpha Glucosidase and Peroxisome proliferator-activated gamma-mediated diabetes. After the investigation in in-vitro, in-vivo, and in silico analysis have confirmed that these phytocompounds can be used as an antidiabetic agent for treating type-2 diabetes mellitus.

5. Conclusion and future perspectives

This present study demonstrated that traditional uses of *Mycetia sinensis* and *Allophylus villosus* by the largest ethnic Chakma community in Bangladesh to treat diabetes led us to discover new anti-hyperglycaemic agents from two Novel plants of Bangladesh with their bioactivities as well as using computer-aided drug development approaches. The scientific evidence for the presence of chemical equivalent of phenolic compounds, and flavonoids performed antioxidant properties of these Noble plants, as well as FTIR analysis confirmed phytochemical functional group contained in both *M. sinensis* & *A. villosus*. GC–MS analysis demonstrated the specific phytochemicals present in these Nobel plants with their molecular weights, chemical identity, and area percentages. In light of the bio-activity study of different fractioned extracts like n-hexane, ethyl acetate, and ethanol extract performed, an oral glucose tolerance test where ethyl acetate and ethanol extracts of *M. sinensis* significantly reduce blood glucose levels and all fractions of *A. villosus* extracts have performed significantly blood reduction compared with control groups on Swiss Albino mice. As significant observations for liver and kidney complications occurred for excess glucose level performed Serum Creatinine and Serum Alkaline Phosphatase tests on Swiss Albino mice. Furthermore, the Computer Aided Drug Development approaches with several parameters demonstrated that the compounds retrieved from these two plants possessed potential antagonist activity against two diabetes metabolic proteins. Correlating the study, the bio-active phytochemicals from *Mycetia sinensis* and *Allophylus villosus* performed antioxidant properties with anti-hyperglycemic activities with no side effects or diabetes complications, as well as inhibitory performance on two diabetes metabolic proteins Alpha-Glucosidase and Peroxisome Proliferator-Activated Receptor Gamma. The study could confirm that these two plants could be non-promising drug sources from nature for the treatment of Diabetes.

Funding

This work was supported by the University Grant Commission (Grant: BMK/Scholarship/Research/College-5/Ph.D/2018/710). Also, the project was also supported by a grant from the Jashore University of Science and Technology (Grant: JUST/Research Cell-112/FoBST-05/2022–23), and Ministry of Science and Technology, Bangladesh (Grant: MoST/2020–21/BS-278).

CRediT authorship contribution statement

Md Nur Kabidul Azam: Data curation, Methodology, Formal analysis, Software, Validation, Investigation, Resources, Writing – original

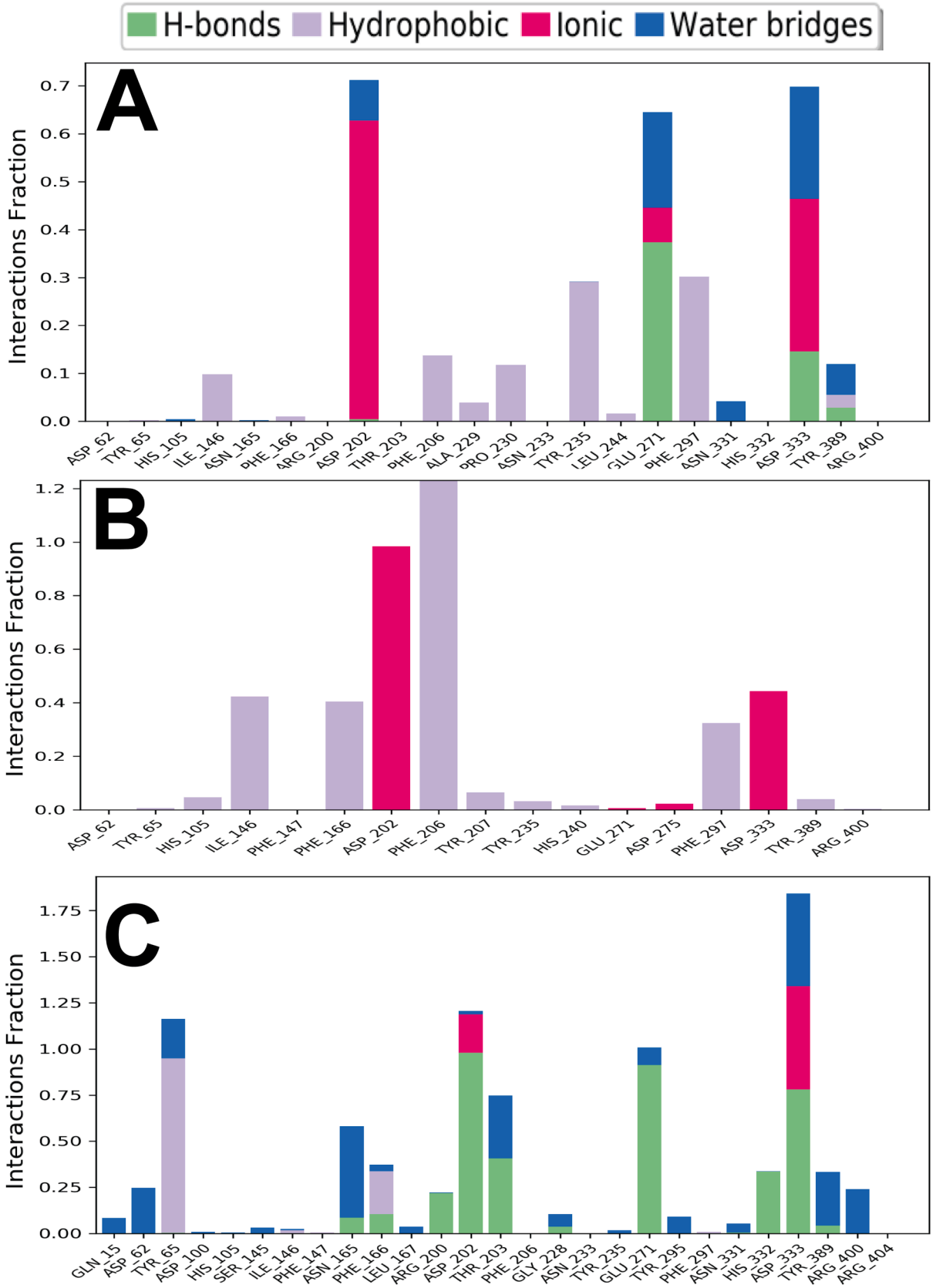

Fig. 9. During the 100 ns simulation duration, the intermolecular interactions between ligands and protein were analysed, as seen in the stacked bar charts. The figure represents the interaction of three ligands with targeted protein human alpha-glucosidase (PDB ID: 3WY1) where (**A**) The Compound CID-102506517, (**B**) CID-6327703 and (**C**) The Control Drug (CID-441314).

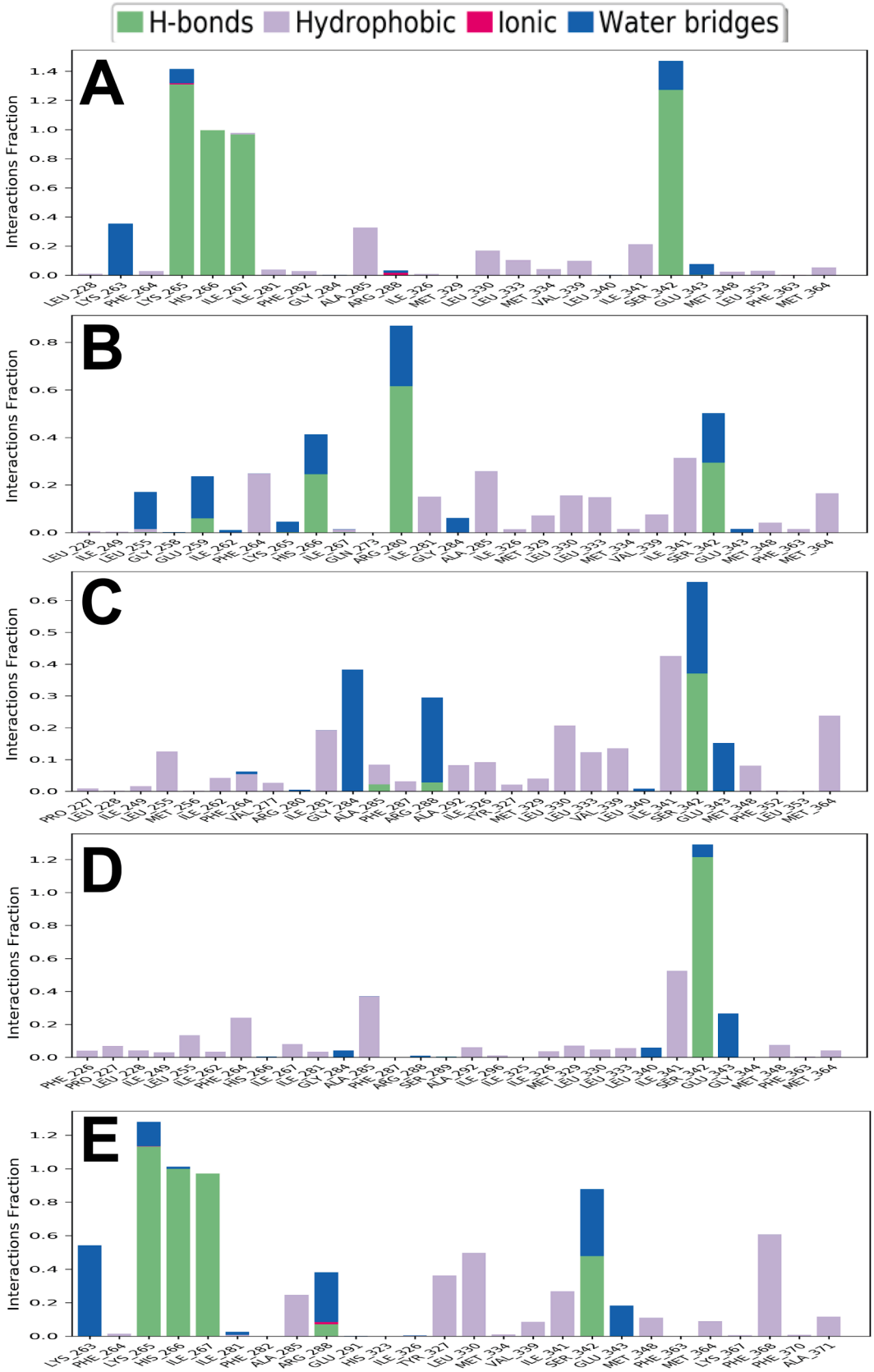

Fig. 10. During the 100 ns simulation duration, the interactions with intramolecular bonds between proteins and ligands were analyzed, as seen in the stacked bar charts. The figure represents the interaction of five ligands with targeted protein peroxisome-activated transcription factor (PDB ID: 8B8Z), where (**A**) The Compound CID-605775, (**B**) CID-605777, (**C**) CID-15764573, (**D**) CID-91720824, (**E**) The Control Drug CID-77999.

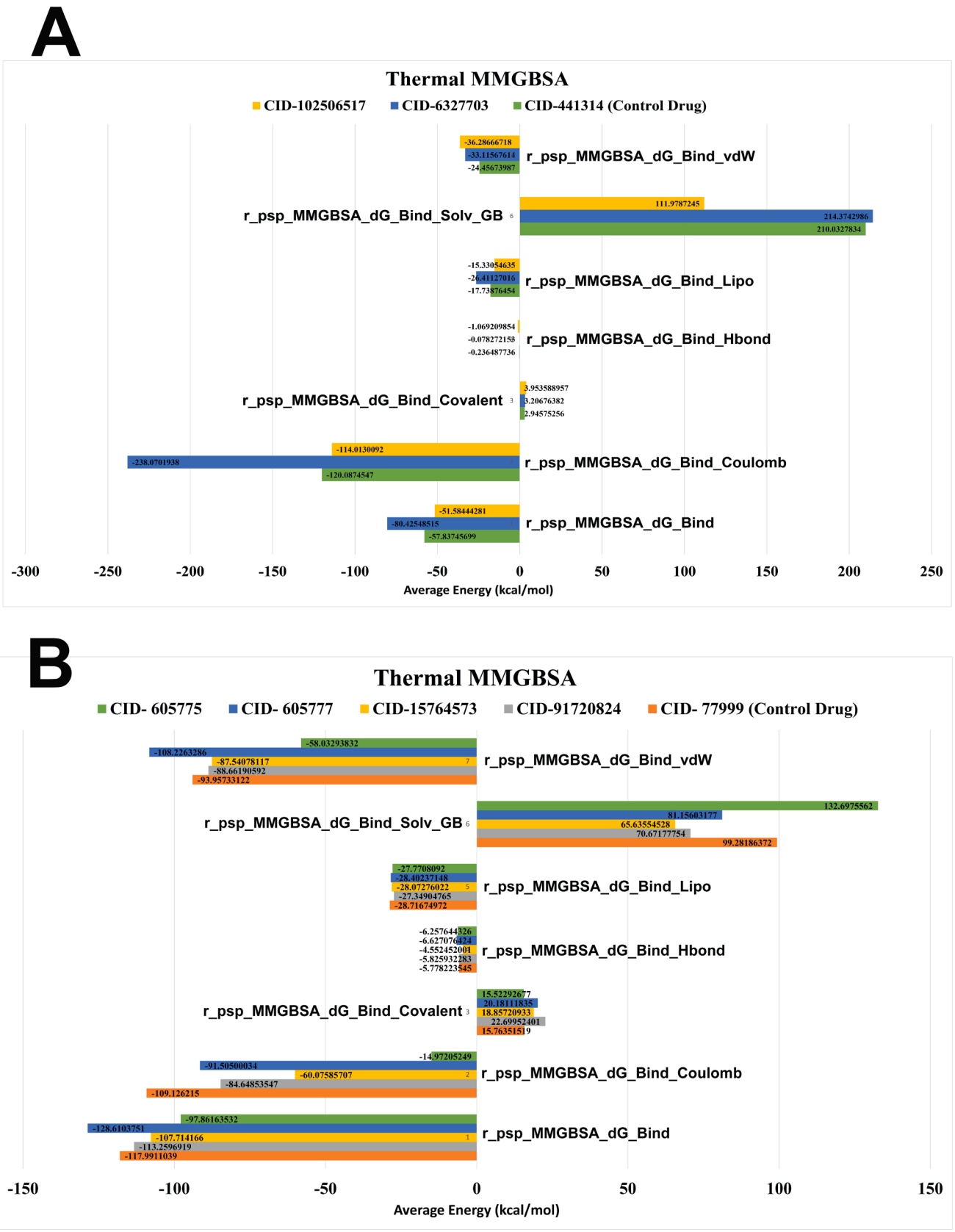

Fig. 11. Post simulation binding free energy (Thermal MMGBSA) calculation of the selected phytocompounds with the targeted proteins. Here, Fig. 11**(A)** -The selected compounds with human alpha-glucosidase (PDB ID: 3WY1); **11(B)** -The chosen compounds with peroxisome-activated transcription factor (PDB ID: 8B8Z).

draft, Visualization, Supervision. **Partha Biswas:** Data curation, Methodology, Formal analysis, Software, Validation, Investigation, Resources, Writing – original draft, Visualization, Supervision. **Md. Mohaimenul Islam Tareq:** Methodology, Formal analysis, Software, Writing – original draft. **Md Ridoy Hossain:** Methodology, Formal analysis, Software, Writing – original draft. **Shabana Bibi:** Validation, Investigation, Writing – original draft, Visualization, Supervision, Funding acquisition. **Md. Anisul Hoque:** Methodology, Formal analysis. **Amia khandker:** Data curation, Writing – original draft. **Md Ashraful Alam:** Methodology, Formal analysis, Validation, Investigation, Resources. **Md. Nazmul Hasan Zilani:** Methodology, Formal analysis, Validation, Investigation, Resources, Visualization, Supervision. **Mohammad Shahedur Rahman:** Validation, Investigation, Resources, Visualization, Supervision. **Norah A. Albekairi:** Validation, Investigation, Visualization, Supervision, Funding acquisition. **Abdulrahman Alshammari:** Validation, Investigation, Visualization, Supervision, Funding acquisition. **Md. Nazmul Hasan:** Validation, Investigation, Resources, Writing – original draft, Visualization, Supervision.

Declaration of competing interest

The authors declare that they have no known competing financial interests or personal relationships that could have appeared to influence the work reported in this paper.

Acknowledgments

Authors are thankful to the Researchers Supporting Project number (RSPD2023R1035), King Saud University, Riyadh, Saudi Arabia. In Addition, 1st Author is also grateful to University Grant Commission, Bangladesh for his scholarship. Authors are pleased on the Department of Pharmacy and the department of Nutrition and Food Technology, Jashore University of Science and Technology, Jashore 7408, Bangladesh. Authors are also grateful for the research facilities at Wazed Miah Science Research Center, Jahangirnagar University, Saver, Dhaka.

Appendix A. Supplementary material

Supplementary data to this article can be found online at https://doi.org/10.1016/j.jsps.2023.101884.

References

Abdullah, A., Biswas, P., Sahabuddin, M., Mubasharah, A., Khan, D.A., Hossain, A., Roy, T., Rafi, N.M.R., Dey, D., Hasan, M., 2023. Molecular dynamics simulation and pharmacoinformatic integrated analysis of bioactive phytochemicals from azadirachta indica (Neem) to treat Diabetes Mellitus. J. Chem. https://doi.org/10.1155/2023/4170703.

Ahmed, H., Mahmud, A.R., Siddiquee, M.F.R., Shahriar, A., Biswas, P., Shimul, M.E.K., Ahmed, S.Z., Ema, T.I., Rahman, N., Khan, M.A., Mizan, M.F.R., Emran, T.B., 2023. Role of T cells in cancer immunotherapy: opportunities and challenges. Cancer Pathogenesis Ther. https://doi.org/10.1016/j.cpt.2022.12.002.

Al Azad, S., Ahmed, S., Biswas, P., Mia, M.A.R., Farjana, M., Arshe, F.A., Mily, S.J., Ankhi, A.B., Shaikat, M.M., Sultana, S., 2022. Quantitative analysis of the factors influencing IDA and TSH downregulation in correlation to the fluctuation of activated vitamin D3 in women. JABET. https://doi.org/10.5455/jabet.2022.d118.

Al Saber, M., Biswas, P., Dey, D., Kaium, M.A., Islam, M.A., Tripty, M.I.A., Rahman, M. H., Rahaman, T.I., Biswas, M.Y., Paul, P., Rahman, M.A., Hasan, M.N., Kim, B., 2022. A comprehensive review of recent advancements in cancer immunotherapy and generation of CAR T Cell by CRISPR-Cas9. Processes 10 (1), 16. https://doi.org/10.3390/pr10010016.

Al-Ishaq, R.K., Abotaleb, M., Kubatka, P., Kajo, K., Büsselberg, D., 2019. Flavonoids and their anti-diabetic effects: cellular mechanisms and effects to improve blood sugar levels. Biomolecules 9 (9). https://doi.org/10.3390/biom9090430.

Altemimi, A., Lakhssassi, N., Baharlouei, A., Watson, D.G., Lightfoot, D.A., 2017. Phytochemicals: extraction, isolation, and identification of bioactive compounds from plant extracts. Plants (Basel) 6 (4). https://doi.org/10.3390/plants6040042.

Andalib, K.M.S., Biswas, P., Sakib, M.R., Hasan, M.N., Rahman, M.H., Habib, A., 2023. Identification of novel MCM2 inhibitors from Catharanthus roseus by pharmacoinformatics, molecular docking and molecular dynamics simulation-based evaluation. Inf. Med. Unlocked 39, 101251. https://doi.org/10.1016/j.imu.2023.101251.

Arefin, A., Ismail Ema, T., Islam, T., Hossen, S., Islam, T., Al Azad, S., Uddin Badal, N., Islam, A., Biswas, P., Alam, N.U., Islam, E., Anjum, M., Masud, A., Kamran, S., Rahman, A., Kumar Paul, P., 2021. Target specificity of selective bioactive compounds in blocking α-dystroglycan receptor to suppress Lassa virus infection: an in silico approach. J. Biomed. Res. 35 (6), 459–473. https://doi.org/10.7555/jbr.35.20210111.

Arman Sharif, M., Mahmud Khan, A., Salekeen, R., Hafijur Rahman, M., Mahmud, S., Bibi, S., Biswas, P., Nazmul Hasan, M., Mohammed Didarul Islam, K., Mahbubur Rahman, S.M., Emdadul Islam, M., Alshammari, A., Alharbi, M., Hayee, A., 2023. Phyllanthus emblica (Amla) methanolic extract regulates multiple checkpoints in 15-Lipoxygenase mediated inflammopathies: computational simulation and in vitro evidence. Saudi Pharm. J. https://doi.org/10.1016/j.jsps.2023.06.014.

Asmilia, N., Fahrimal, Y., Abrar, M., Rinidar, R., 2020. Chemical compounds of Malacca leaf (Phyllanthus emblica) after triple extraction with n-hexane, ethyl acetate, and ethanol. Sci. World J. 2020, 2739056. https://doi.org/10.1155/2020/2739056.

Azam, M.N.K., Shishir, T.A., Khandker, A., Hasan, M.N. 2022. Value-added products from industrial wastes of phytopharmaceutical industries. In: Innovations in Fermentation and Phytopharmaceutical Technologies. Elsevier, pp. 457-489. https://doi.org/10.1016/B978-0-12-821877-8.00002-6.

Babbar, N., Oberoi, H.S., Sandhu, S.K., Bhargav, V.K., 2014. Influence of different solvents in extraction of phenolic compounds from vegetable residues and their evaluation as natural sources of antioxidants. J. Food Sci. Technol. 51 (10), 2568–2575. https://doi.org/10.1007/s13197-012-0754-4.

Baehaki, A., Lestari, S., Hendri, M., Ariska, F., 2020a. Antidiabetic activity with n-hexane, ethyl-acetate and ethanol extract of Halodule uninervis seagrass. Pharmacognosy J. 12 (4) https://doi.org/10.5530/pj.2020.12.115.

Baehaki, A., Lestari, S., Hendri, M., Ariska, F.J.P.J., 2020b. Antidiabetic activity with n-hexane, ethyl-acetate and ethanol extract of Halodule uninervis seagrass. Pharmacognosy J. 12 (4) https://doi.org/10.5530/pj.2020.12.115.

Ban, T., Ohue, M., Akiyama, Y., 2018. Multiple grid arrangement improves ligand docking with unknown binding sites: application to the inverse docking problem. Comput. Biol. Chem. 73, 139–146. https://doi.org/10.1016/j.compbiolchem.2018.02.008.

Bari, M.W., Islam, M.M., Khatun, M., Sultana, M.J., Ahmed, R., Islam, A., Hossain, M.I., Rahman, M.M., Islam, M.A.J.C.P., 2020. Antidiabetic effect of Wedelia chinensis leaf extract in alloxan induced Swiss albino diabetic mice. Clin. Phytosci. 6 (1), 1–8. https://doi.org/10.1186/s40816-020-00197-6.

Barrett-Connor, E., 2003. Diabetes and heart disease. Diabetes Care 26 (10), 2947–2958. https://doi.org/10.2337/diacare.26.10.2947.

Becke, A.D., 1988. Density-functional exchange-energy approximation with correct asymptotic behavior. Phys. Rev. A Gen. Phys. 38 (6), 3098–3100. https://doi.org/10.1103/physreva.38.3098.

Benedé-Ubieto, R., Estévez-Vázquez, O., Ramadori, P., Cubero, F.J., Nevzorova, Y.A., 2020. Guidelines and considerations for metabolic tolerance tests in mice. Diabetes Metab. Syndr. Obes. 13, 439–450. https://doi.org/10.2147/dmso.S234665.

Bermúdez, V., Finol, F., Parra, N., Parra, M., Pérez, A., Peñaranda, L., Vílchez, D., Rojas, J., Arráiz, N., Velasco, M., 2010. PPAR-gamma agonists and their role in type 2 diabetes mellitus management. Am. J. Ther. 17 (3), 274–283. https://doi.org/10.1097/MJT.0b013e3181c08081.

Bharadwaj, S., Dubey, A., Yadava, U., Mishra, S.K., Kang, S.G., Dwivedi, V.D., 2021. Exploration of natural compounds with anti-SARS-CoV-2 activity via inhibition of SARS-CoV-2 Mpro. Brief Bioinform. 22 (2), 1361–1377. https://doi.org/10.1093/bib/bbaa382.

Bharat, C.R., Krishna, G.D., 2017. GC-MS analysis of young leaves of allophylus cobbe (L.) raeusch and allophylus serratus (Roxb.) Kurz. Indian J. Pharm. Educat. Res. 51 (3), 472–479. https://doi.org/10.5530/ijper.51.3.75.

Bhat, S. G. 2021a. Medicinal Plants and Its Pharmacological Values. In: Natural Medicinal Plants. IntechOpen London, UK.

Bhat, S. G. 2021b. Medicinal plants and its pharmacological values. Natural Medicinal Plants.

Biswas, P., Dey, D., Biswas, P.K., Rahaman, T.I., Saha, S., Parvez, A., Khan, D.A., Lily, N. J., Saha, K., Sohel, M., Hasan, M.M., Al Azad, S., Bibi, S., Hasan, M.N., Rahmatullah, M., Chun, J., Rahman, M.A., Kim, B., 2022a. A Comprehensive analysis and anti-cancer activities of quercetin in ROS-mediated cancer and cancer stem cells. Int. J. Mol. Sci. 23 (19) https://doi.org/10.3390/ijms231911746.

Biswas, P., Hany Rumi, O., Ahmed Khan, D., Ahmed, M.N., Nahar, N., Jahan, R., Hasan Zilani, M.N., Paul, T.K., Hasan, A., Bondhon, T.A., Jannat, K., Hasan, M.N., Rahmatullah, M., 2022b. Evaluation of melongosides as potential inhibitors of NS2B-NS3 activator-protease of dengue virus (Serotype 2) by using molecular docking and dynamics simulation approach. J. Trop Med. 2022, 7111786. https://doi.org/10.1155/2022/7111786.

Biswas, P., Bibi, S., Yousafi, Q., Mehmood, A., Saleem, S., Ihsan, A., Dey, D., Hasan Zilani, M.N., Hasan, M.N., Saleem, R., Awaji, A.A., Fahmy, U.A., Abdel-Daim, M.M., 2023a. Study of MDM2 as prognostic biomarker in Brain-LGG cancer and bioactive phytochemicals inhibit the p53-MDM2 pathway: a computational drug development approach. Molecules 28 (7). https://doi.org/10.3390/molecules28072977.

Biswas, P., Polash, S.A., Dey, D., Kaium, M.A., Mahmud, A.R., Yasmin, F., Baral, S.K., Islam, M.A., Rahaman, T.I., Abdullah, A., Ema, T.I., Khan, D.A., Bibi, S., Chopra, H., Kamel, M., Najda, A., Fouda, M.M.A., Rehan, U.M., Mheidat, M., Alsaidalani, R., Abdel-Daim, M.M., Hasan, M.N., 2023b. Advanced implications of nanotechnology in disease control and environmental perspectives. Biomed. Pharmacother. 158, 114172 https://doi.org/10.1016/j.biopha.2022.114172.

Brogi, S., Ramalho, T.C., Kuca, K., Medina-Franco, J.L., Valko, M., 2020. In silico methods for drug design and discovery. In: Vol. 8. Frontiers Media SA, pp. 612.

Chavan, R., Gaikwad, D., 2016. The ethnobotany, phytochemistry and biological properties of Allophylus species used in traditional medicine: a review. World J. Pharm. Pharm. Sci. 5 (11), 664–682. https://doi.org/10.20959/wjpps201611-8039.
Chowdhury, M.A.B., Islam, M., Rahman, J., Uddin, M.J., Haque, M.R., 2022. Diabetes among adults in Bangladesh: changes in prevalence and risk factors between two cross-sectional surveys. BMJ Open 12 (8), e055044.
Dada-Adegbola, H., Moody, J., 2022. In vitro activities of the methanolic extracts and fractions of Bridelia ferruginea Benth on clinical isolates of multidrug resistant gram-negative bacteria. J. Pharmacognosy Phytochem. 11 (4), 01–09. https://doi.org/10.22271/phyto.2022.v11.i4a.14437.
David, T.I., Adelakun, N.S., Omotuyi, O.I., Metibemu, D.S., Ekun, O.E., Inyang, O.K., Adewumi, B., Enejoh, O.A., Owolabi, R.T., Oribamise, E.I., 2018. Molecular docking analysis of phyto-constituents from Cannabis sativa with pfDHFR. Bioinformation 14 (9), 574.
Deka, H., Choudhury, A., Dey, B.K., 2022. An overview on plant derived phenolic compounds and their role in treatment and management of diabetes. J Pharmacopuncture 25 (3), 199–208. https://doi.org/10.3831/kpi.2022.25.3.199.
Derosa, G., Maffioli, P., 2012. Peroxisome proliferator-activated receptor-γ (PPAR-γ) agonists on glycemic control, lipid profile and cardiovascular risk. Curr. Mol. Pharmacol. 5 (2), 272–281.
Dev, S., 1997. Ethnotherapeutics and modern drug development: the potential of Ayurveda. Curr. Sci. 73 (11), 909–928.
Dey, D., Biswas, P., Paul, P., Mahmud, S., Ema, T.I., Khan, A.A., Ahmed, S.Z., Hasan, M. M., Saikat, A.S.M., Fatema, B., Bibi, S., Rahman, M.A., Kim, B., 2022a. Natural flavonoids effectively block the CD81 receptor of hepatocytes and inhibit HCV infection: a computational drug development approach. Mol Divers. https://doi.org/10.1007/s11030-022-10491-9.
Dey, D., Hossain, R., Biswas, P., Paul, P., Islam, M.A., Ema, T.I., Gain, B.K., Hasan, M.M., Bibi, S., Islam, M.T., Rahman, M.A., Kim, B., 2022b. Amentoflavone derivatives significantly act towards the main protease (3CL(PRO)/M(PRO)) of SARS-CoV-2: in silico admet profiling, molecular docking, molecular dynamics simulation, network pharmacology. Mol Divers 1–15. https://doi.org/10.1007/s11030-022-10459-9.
Dong, J., Wang, N.-N., Yao, Z.-J., Zhang, L., Cheng, Y., Ouyang, D., Lu, A.-P., Cao, D.-S., 2018. ADMETlab: a platform for systematic ADMET evaluation based on a comprehensively collected ADMET database. J. Cheminformatics 10, 1–11.
Doughari, J.H., 2012. Phytochemicals: extraction methods, basic structures and mode of action as potential chemotherapeutic agents. INTECH Open Access Publisher Rijeka, Croatia.
Ekor, M., 2014. The growing use of herbal medicines: issues relating to adverse reactions and challenges in monitoring safety. Front Pharmacol 4, 177. https://doi.org/10.3389/fphar.2013.00177.
Erejuwa, O.O., Sulaiman, S.A., Wahab, M.S.A., Sirajudeen, K.N.S., Salleh, M.S.M., Gurtu, S., 2010. Antioxidant protective effect of glibenclamide and metformin in combination with honey in pancreas of streptozotocin-induced diabetic rats. Int. J. Mol. Sci. 11, 2056–2066.
Fabricant, D.S., Farnsworth, N.R., 2001. The value of plants used in traditional medicine for drug discovery. Environ Health Perspect 109 (Suppl 1), 69–75. https://doi.org/10.1289/ehp.01109s169.
Fatima, H., Shahid, M., Jamil, A., Naveed, M., 2021. Therapeutic potential of selected medicinal plants against carrageenan induced inflammation in rats. Dose Response 19 (4), 15593258211058028. https://doi.org/10.1177/15593258211058028.
Felisbino, K., Granzotti, J.G., Bello-Santos, L., Guiloski, I.C., 2021. Nutrigenomics in regulating the expression of genes related to Type 2 Diabetes Mellitus. Front Physiol 12, 699220. https://doi.org/10.3389/fphys.2021.699220.
Fenercioglu, A.K., Saler, T., Genc, E., Sabuncu, H., Altuntas, Y., 2010. The effects of polyphenol-containing antioxidants on oxidative stress and lipid peroxidation in Type 2 diabetes mellitus without complications. J. Endocrinol. Invest. 33 (2), 118–124. https://doi.org/10.1007/bf03346565.
Ferdausi, N., Islam, S., Rimti, F.H., Quayum, S.T., Arshad, E.M., Ibnat, A., Islam, T., Arefin, A., Ema, T.I., Biswas, P., Dey, D., Azad, S.A., 2022. Point-specific interactions of isovitexin with the neighboring amino acid residues of the hACE2 receptor as a targeted therapeutic agent in suppressing the SARS-CoV-2 influx mechanism. J. Adv. Vet. Anim. Res. 9 (2), 230–240. https://doi.org/10.5455/javar.2022.i588.
Feudjio, C., Yameen, M.A., Singor Njateng, G.S., Khan, M.A., Lacmata Tamekou, S., Simo Mpetga, J.D., Kuiate, J.R., 2020. The influence of solvent, host, and phenological stage on the yield, chemical composition, and antidiabetic and antioxidant properties of Phragmanthera capitata (Sprengel) S. Balle. Evid. Based Complement. Alternat Med. 2020, 6284925. https://doi.org/10.1155/2020/6284925.
Florez, J.C., Jablonski, K.A., Sun, M.W., Bayley, N., Kahn, S.E., Shamoon, H., Hamman, R.F., Knowler, W.C., Nathan, D.M., Altshuler, D., 2007. Effects of the type 2 diabetes-associated PPARG P12A polymorphism on progression to diabetes and response to troglitazone. J. Clin. Endocrinol. Metab. 92 (4), 1502–1509. https://doi.org/10.1210/jc.2006-2275.
Friesner, R.A., Guallar, V., 2005. Ab initio quantum chemical and mixed quantum mechanics/molecular mechanics (QM/MM) methods for studying enzymatic catalysis. Annu. Rev. Phys. Chem. 56, 389–427. https://doi.org/10.1146/annurev.physchem.55.091602.094410.
Gamboa-Antiñolo, F.-M., 2023. Diabetic foot ulcers: a growing global health emergency in the COVID-19 era. Intern. Emerg. Med. 1–3. https://doi.org/10.1007/s11739-023-03217-8.
Gazor, R., Asgari, M., Pasdaran, A., Mohammadghasemi, F., Nasiri, E., Atrkar Roushan, Z., 2017. Evaluation of hepatoprotective effect of acantholimon gilliati eerial part methanolic extract. Iran J. Pharm. Res. 16 (Suppl), 135–141.
Grant-Peters, M., Rich-Griffin, C., Grant-Peters, J.E., Cinque, G., Dendrou, C.A., 2022. Photizo: an open-source library for cross-sample analysis of FTIR spectroscopy data. Bioinformatics 38 (13), 3490–3492. https://doi.org/10.1093/bioinformatics/btac346.
Grover, J.K., Yadav, S.P., Vats, V., 2003a. Effect of feeding Murraya koeingii and Brassica juncea diet kidney functions and glucose levels in streptozotocin diabetic mice. J. Ethnopharmacol. 85 (1), 1–5. https://doi.org/10.1016/S0378-8741(02)00355-0.
Grover, J.K., Yadav, S.P., Vats, V., 2003b. Effect of feeding Murraya koeingii and Brassica juncea diet on [correction] kidney functions and glucose levels in streptozotocin diabetic mice. J. Ethnopharmacol. 85 (1), 1–5. https://doi.org/10.1016/s0378-8741(02)00355-0.
Hasan, A., Biswas, P., Bondhon, T.A., Jannat, K., Paul, T.K., Paul, A.K., Jahan, R., Nissapatorn, V., Mahboob, T., Wilairatana, P., Hasan, M.N., de Lourdes Pereira, M., Wiart, C., Rahmatullah, M., 2022a. Can artemisia herba-alba be useful for managing COVID-19 and comorbidities? Molecules 27 (2). https://doi.org/10.3390/molecules27020492.
Hasan, M.M., Zilani, M.N.H., Akter, S., Nasrin, P., Shajib, G.M.A., Islam, M.A., Biswas, P., Mahmud, S., Saleh, M.A., Hasan, M.N., Uddin, S.J., Shilpi, J.A., 2022b. UHPLC-Q/Orbitrap/MS based chemical fingerprinting and hepatoprotective potential of a medicinal plant, Morinda angustifolia Roxb. S. Afr. J. Bot. 148, 561–572. https://doi.org/10.1016/j.sajb.2022.05.037.
Hasibuzzaman, M., Alam, H., Mia, M., Islam, S., Sultana, S., Ahmed, S., Masud, A., Rahman, S., Khan, A., Rimti, F., Pyash, A., Biswas, P., Shoshi, H., Siddiquy, M., Rimu, F., Zaman, R., Habiba, M., 2023. Serological and oncoinformatic analysis of HbA1c as a prognostic bioma rker in screening the risks of different cancers among the male T2D pa tients of Bangladesh. J. Adv. Biotechnol. Experimental Ther. 6 (2), 510. https://doi.org/10.5455/jabet.2023.d145.
Jabin, A., Uddin, M.F., Al Azad, S., Rahman, A., Tabassum, F., Sarker, P., Morshed, A.K. M.H., Rahman, S., Raisa, F.F., Sakib, M.R., Olive, A.H., Islam, T., Tahsin, R., Ahmed, S.Z., Biswas, P., Habiba, M.U., Siddiquy, M., Jafary, M., 2023. Target-specificity of different amyrin subunits in impeding HCV influx mechanism inside the human cells considering the quantum tunnel profiles and molecular strings of the CD81 receptor: a combined in silico and in vivo study. In Silico Pharmacol. 11 (1), 8. https://doi.org/10.1007/s40203-023-00144-6.
Karim, M.A., Islam, M.A., Islam, M.M., Rahman, M.S., Sultana, S., Biswas, S., Hosen, M. J., Mazumder, K., Rahman, M.M., Hasan, M.N., 2020a. Evaluation of antioxidant, anti-hemolytic, cytotoxic effects and anti-bacterial activity of selected mangrove plants (Bruguiera gymnorrhiza and Heritiera littoralis) in Bangladesh. Clin. Phytosci. 6 (1), 1–12. https://doi.org/10.1186/s40816-020-0152-9.
Karim, M.A., Islam, M.A., Islam, M.M., Rahman, M.S., Sultana, S., Biswas, S., Hosen, M. J., Mazumder, K., Rahman, M.M., Hasan, M.N.J.C.P., 2020b. Evaluation of antioxidant, anti-hemolytic, cytotoxic effects and anti-bacterial activity of selected mangrove plants (Bruguiera gymnorrhiza and Heritiera littoralis) in Bangladesh. Clin. Phytosci. 6 (1), 1–12. https://doi.org/10.1186/s40816-020-0152-9.
Kelly, J.P., Kaufman, D.W., Kelley, K., Rosenberg, L., Anderson, T.E., Mitchell, A.A., 2005. Recent trends in use of herbal and other natural products. Arch. Intern. Med. 165 (3), 281–286. https://doi.org/10.1001/archinte.165.3.281.
Khan, R.A., Hossain, R., Siyadatpanah, A., Al-Khafaji, K., Khalipha, A.B.R., Dey, D., Asha, U.H., Biswas, P., Saikat, A.S.M., Chenari, H.A., Wilairatana, P., Islam, M.T., 2021. Diterpenes/Diterpenoids and their derivatives as potential bioactive leads against Dengue virus: a computational and network pharmacology study. Molecules 26 (22). https://doi.org/10.3390/molecules26226821.
Khan, A.M., Sharif, M.A., Salekeen, R., Rahman, M.H., Mahmud, S., Biswas, P., Hasan, M. N., Islam, K.M.D., Billah, M.M., Islam, M.E., 2023. In vitro and in silico investigation of garlic's (Allium sativum) bioactivity against 15-lipoxygenase mediated inflammopathies. J. Herbmed Pharmacol. 12 (2), 283–298. https://doi.org/10.34172/jhp.2023.31.
Kumar, S., Egbuna, C., 2019. Phytochemistry: an in-Silico and in-Vitro Update. Springer.
Küme, T., Sağlam, B., Ergon, C., Sisman, A.R., 2018. Evaluation and comparison of Abbott Jaffe and enzymatic creatinine methods: could the old method meet the new requirements? J Clin Lab Anal 32 (1). https://doi.org/10.1002/jcla.22168.
Lee, C., Yang, W., Parr, R.G., 1988. Development of the Colle-Salvetti correlation-energy formula into a functional of the electron density. Phys. Rev. B Condens. Matter 37 (2), 785–789. https://doi.org/10.1103/physrevb.37.785.
Lila, M.A., Raskin, I., 2005. Health-related interactions of phytochemicals. J. Food Sci. 70 (1), R20–R27. https://doi.org/10.1111/j.1365-2621.2005.tb09054.x.
Ling, W., Huang, Y., Huang, Y.M., Fan, R.R., Sui, Y., Zhao, H.L., 2020. Global trend of diabetes mortality attributed to vascular complications, 2000–2016. Cardiovasc. Diabetol. 19 (1), 182. https://doi.org/10.1186/s12933-020-01159-5.
Lu, X., Chen, H., Dong, P., Fu, L., Zhang, X., 2010. Phytochemical characteristics and hypoglycaemic activity of fraction from mushroom Inonotus obliquus. J. Sci. Food Agric. 90 (2), 276–280. https://doi.org/10.1002/jsfa.3809.
Lu, G., Shrestha, B., Haes, A.J., 2016. Importance of tilt angles of adsorbed aromatic molecules on nanoparticle rattle SERS substrates. J. Phys. Chem. C 120 (37), 20759–20767. https://doi.org/10.1021/acs.jpcc.6b02023.
Mahnashi, M.H., Alqahtani, Y.S., Alyami, B.A., Alqarni, A.O., Ayaz, M., Ghufran, M., Ullah, F., Sadiq, A., Ullah, I., Haq, I.U., Khalid, M., Murthy, H.C.A., 2022. Phytochemical analysis, α-Glucosidase and amylase inhibitory, and molecular docking studies on Persicaria hydropiper L. leaves essential oils. Evid. Based Complement. Alternat. Med., 7924171 https://doi.org/10.1155/2022/7924171.
Maobe, M.A.G., Gitu, L., Gatebe, E., 2021. Evaluation of antibacterial and antifungal activity of herbs used in treatment of diabetes, malaria and pneumonia in Kisii and Nyamira counties Region, Kenya. J. Tropical Pharm. Chem. 5 (4), 330–337. https://doi.org/10.25026/jtpc.v5i4.314.
Mihailović, M., Dinić, S., Arambašić Jovanović, J., Uskoković, A., Grdović, N., Vidaković, M., 2021. The influence of plant extracts and phytoconstituents on antioxidant enzymes activity and gene expression in the prevention and treatment of

impaired glucose homeostasis and diabetes complications. Antioxidants (Basel) 10 (3). https://doi.org/10.3390/antiox10030480.
Murugan, D.D., Balan, D., Wong, P.F., 2021. Adipogenesis and therapeutic potentials of antiobesogenic phytochemicals: Insights from preclinical studies. Phytother. Res. 35 (11), 5936–5960. https://doi.org/10.1002/ptr.7205.
Nakamura, M., Ra, J.H., Jee, Y., Kim, J.S., 2017. Impact of different partitioned solvents on chemical composition and bioavailability of Sasa quelpaertensis Nakai leaf extract. J. Food Drug Anal. 25 (2), 316–326. https://doi.org/10.1016/j.jfda.2016.08.006.
Pal, A., McCarthy, M.I., 2013. The genetics of type 2 diabetes and its clinical relevance. Clin. Genet. 83 (4), 297–306. https://doi.org/10.1111/cge.12055.
Pan, S.Y., Litscher, G., Gao, S.H., Zhou, S.F., Yu, Z.L., Chen, H.Q., Zhang, S.F., Tang, M. K., Sun, J.N., Ko, K.M., 2014. Historical perspective of traditional indigenous medical practices: the current renaissance and conservation of herbal resources. Evid. Based Complement. Alternat. Med. 2014, 525340 https://doi.org/10.1155/2014/525340.
Pandey, A., Tripathi, S., 2014. Concept of standardization, extraction and pre phytochemical screening strategies for herbal drug. J. Pharmacognosy Phytochem. 2 (5), 115–119.
Paramasivam, D., Safi, S.Z., Qvist, R., Abidin, I.B.Z., Hairi, N.N.M., Chinna, K., 2016. Role of PPARG (Pro12Ala) in Malaysian type 2 diabetes mellitus patients. Int. J. Diabetes Dev. Countries 36, 449–456. https://doi.org/10.1007/s13410-015-0462-5.
Parr, R.G. 1980. Density functional theory of atoms and molecules. Horizons of Quantum Chemistry: Proceedings of the Third International Congress of Quantum Chemistry Held at Kyoto, Japan, October 29-November 3, 1979.
Paul, P.K., Al Azad, S., Rahman, M.H., Farjana, M., Uddin, M.R., Dey, D., Mahmud, S., Ema, T.I., Biswas, P., Anjum, M., Akhi, O.J., Ahmed, S.Z., 2022. Catabolic profiling of selective enzymes in the saccharification of non-food lignocellulose parts of biomass into functional edible sugars and bioenergy: an in silico bioprospecting. J. Adv. Vet. Anim. Res. 9 (1), 19–32. https://doi.org/10.5455/javar.2022.i565.
Pearson, R.G., 1986. Absolute electronegativity and hardness correlated with molecular orbital theory. Proc. Natl. Acad. Sci. U.S.A. 83 (22), 8440–8441. https://doi.org/10.1073/pnas.83.22.8440.
Proença, C., Freitas, M., Ribeiro, D., Oliveira, E.F.T., Sousa, J.L.C., Tomé, S.M., Ramos, M.J., Silva, A.M.S., Fernandes, P.A., Fernandes, E., 2017. α-Glucosidase inhibition by flavonoids: an in vitro and in silico structure-activity relationship study. J. Enzyme Inhib. Med. Chem. 32 (1), 1216–1228. https://doi.org/10.1080/14756366.2017.1368503.
Proestos, C., Komaitis, M., 2013. Analysis of naturally occurring phenolic compounds in aromatic plants by RP-HPLC Coupled to Diode Array Detector (DAD) and GC-MS after silylation. Foods 2 (1), 90–99. https://doi.org/10.3390/foods2010090.
Proestos, C., Sereli, D., Komaitis, M.J.F.C., 2006. Determination of phenolic compounds in aromatic plants by RP-HPLC and GC-MS. Food Chem. 95 (1), 44–52. https://doi.org/10.1016/j.foodchem.2004.12.016.
Rahman, M.D.H., Biswas, P., Dey, D., Hannan, M.A., Sahabuddin, M., Araf, Y., Kwon, Y., Emran, T.B., Ali, M.S., Uddin, M.J., 2022. An in-silico identification of potential flavonoids against kidney fibrosis targeting TGFβR-1. Life (Basel) 12 (11). https://doi.org/10.3390/life12111764.
Rahman, M.A., Rahman, M.D.H., Hossain, M.S., Biswas, P., Islam, R., Uddin, M.J., Rahman, M.H., Rhim, H., 2020a. Molecular insights into the multifunctional role of natural compounds: autophagy modulation and cancer prevention. Biomedicines 8 (11). https://doi.org/10.3390/biomedicines8110517.
Rahman, M.A., Rahman, M.H., Biswas, P., Hossain, M.S., Islam, R., Hannan, M.A., Uddin, M.J., Rhim, H., 2020b. Potential therapeutic role of phytochemicals to mitigate mitochondrial dysfunctions in Alzheimer's disease. Antioxidants (Basel) 10 (1). https://doi.org/10.3390/antiox10010023.
Rahman, M.S., Zilani, M.N.H., Islam, M.A., Hasan, M.M., Islam, M.M., Yasmin, F., Biswas, P., Hirashima, A., Rahman, M.A., Hasan, M.N.J.P., 2021. In vivo Neuropharmacological potential of Gomphandra tetrandra (Wall.) sleumer and in-silico study against β-amyloid precursor protein. Processes 9 (8), 1449. https://doi.org/10.3390/pr9081449.
Rahmatullah, M., Azam, M.N.K., Pramanik, S., Sania, S.R., Jahan, R., 2012a. Antihyperglycemic activity evaluation of rhizomes of Curcuma zedoaria Christm. roscoe and fruits of Sonneratia caseolaris L. Engl. Int. J. PharmTech Res. 4 (1), 125–129.
Rahmatullah, M., Chowdhury, A.R., Esha, R.T., Chowdhury, M.R., Adhikary, S., Haque, K.M.A., Paul, A., Akber, M., 2012b. Ayurvedic influence on use of medicinal plants in Chakma traditional medicine. Am. Eurasian J. Sustain. Agric. 6, 107–112.
Raies, A.B., Bajic, V.B., 2016. In silico toxicology: computational methods for the prediction of chemical toxicity. Computational Mol. Sci. 6 (2), 147–172.
Ramírez-Alarcón, K., Victoriano, M., Mardones, L., Villagran, M., Al-Harrasi, A., Al-Rawahi, A., Cruz-Martins, N., Sharifi-Rad, J., Martorell, M., 2021. Phytochemicals as potential epidrugs in Type 2 Diabetes Mellitus. Front. Endocrinol. (Lausanne) 12, 656978. https://doi.org/10.3389/fendo.2021.656978.
Roos, K., Wu, C., Damm, W., Reboul, M., Stevenson, J.M., Lu, C., Dahlgren, M.K., Mondal, S., Chen, W., Wang, L., Abel, R., Friesner, R.A., Harder, E.D., 2019. OPLS3e: extending force field coverage for drug-like small molecules. J. Chem. Theory Comput. 15 (3), 1863–1874. https://doi.org/10.1021/acs.jctc.8b01026.
Roth, G., 2018. Global Burden of Disease Collaborative Network. Global Burden of Disease Study 2017 (GBD 2017) Results. Seattle, United States: Institute for Health Metrics and Evaluation (IHME), 2018. Lancet 392, 1736–1788.
Saha, A., Marma, K.K.S., Rashid, A., Tarannum, N., Das, S., Chowdhury, T., Afrin, N., Chakraborty, P., Emran, M., Mehedi, H.M.H., Hussain, M.I., Barua, A., Mistry, S.K., 2022. Risk factors associated with self-medication among the indigenous communities of Chittagong Hill Tracts, Bangladesh. PLoS One 17 (6), e0269622. https://doi.org/10.1371/journal.pone.0269622.
Saifuddin, A., Mahbub, R., Akter, S., Fardous, J., 2017. Infrared spectroscopy study of the ethanolic leaf extracts of Artocarpus heterophyllus and Litchi chinensis. MOJ Appl. Bionics Biomech. https://doi.org/10.15406/mojabb. 2017.01. 00029.
Salam, N.K., Huang, T.H., Kota, B.P., Kim, M.S., Li, Y., Hibbs, D.E., 2008. Novel PPAR-gamma agonists identified from a natural product library: a virtual screening, induced-fit docking and biological assay study. Chem. Biol. Drug Des. 71 (1), 57–70. https://doi.org/10.1111/j.1747-0285.2007.00606.x.
Sarhangi, N., Sharifi, F., Hashemian, L., Hassani Doabsari, M., Heshmatzad, K., Rahbaran, M., Jamaldini, S.H., Aghaei Meybodi, H.R., Hasanzad, M., 2020. PPARG (Pro12Ala) genetic variant and risk of T2DM: a systematic review and meta-analysis. Sci. Rep. 10 (1), 12764. https://doi.org/10.1038/s41598-020-69363-7.
Sarker, M.T., Saha, S., Biswas, P., Islam, M.T., Sheikh, M.A., Hasan, M.N., Islam, N., Rabbe, M.M.I., Rafi, M.O., 2022. Identification of blood-based inflammatory biomarkers for the early-stage detection of acute myocardial infarction. Network Modeling Anal. Health Informatics Bioinform. 11 (1), 28. https://doi.org/10.1007/s13721-022-00371-5.
Sathish Kumar, S.R., Bhaskara Rao, K.V., 2016. Postprandial anti-hyperglycemic activity of marine Streptomyces coelicoflavus SRBVIT13 mediated gold nanoparticles in streptozotocin induced diabetic male albino Wister rats. IET Nanobiotechnol. 10 (5), 308–314. https://doi.org/10.1049/iet-nbt.2015.0094.
Shiau, A.K., Barstad, D., Loria, P.M., Cheng, L., Kushner, P.J., Agard, D.A., Greene, G.L., 1998. The structural basis of estrogen receptor/coactivator recognition and the antagonism of this interaction by tamoxifen. Cell 95 (7), 927–937. https://doi.org/10.1016/s0092-8674(00)81717-1.
Simorangkir, M., Nainggolan, B., Silaban, S. 2019. Secondary metabolites phytochemical analysis of n-Hexane, ethyl acetate and ethanol extracts of Sarang banua (Clerodendrum fragrans Vent Willd) leaves. In: AISTSSE 2018: Proceedings of The 5th Annual International Seminar on Trends in Science and Science Education, AISTSSE 2018, 18-19 October 2018, Medan, Indonesia.
Singh, S., Sharma, B., Kanwar, S.S., Kumar, A., 2016. Lead phytochemicals for anticancer drug development. Front. Plant Sci. 7, 1667. https://doi.org/10.3389/fpls.2016.01667.
Socrates, G., 2004. Infrared and Raman Characteristic Group Frequencies: Tables and Charts. John Wiley & Sons.
Sohel, M., Biswas, P., Al Amin, M., Hossain, M.A., Sultana, H., Dey, D., Aktar, S., Setu, A., Khan, M.S., Paul, P., Islam, M.N., Rahman, M.A., Kim, B., Al Mamun, A., 2022. Genistein, a potential phytochemical against breast cancer treatment-insight into the molecular mechanisms. Processes 10 (2), 415. https://doi.org/10.3390/pr10020415.
Sohel, M., Aktar, S., Biswas, P., Amin, M.A., Hossain, M.A., Ahmed, N., Mim, M.I.H., Islam, F., Mamun, A.A., 2023. Exploring the anti-cancer potential of dietary phytochemicals for the patients with breast cancer: a comprehensive review. Cancer Med. 1–28. https://doi.org/10.1002/cam4.5984.
Swargiary, A., Roy, M.K., Mahmud, S., 2023. Phenolic compounds as α-glucosidase inhibitors: a docking and molecular dynamics simulation study. J. Biomol. Struct. Dyn. 41 (9), 3862–3871. https://doi.org/10.1080/07391102.2022.2058092.
Tiji, S., Bouhrim, M., Addi, M., Drouet, S., Lorenzo, J.M., Hano, C., Bnouham, M., Mimouni, M., 2021. Linking the phytochemicals and the α-glucosidase and α-amylase enzyme inhibitory effects of Nigella sativa seed extracts. Foods 10 (8). https://doi.org/10.3390/foods10081818.
Tittikpina, N.K., Kirsch, G., Duval, R.E., Chaimbault, P., Jacob, C., 2022. Daniellia oliveri (Rolfe) Hutch and Dalziel: antimicrobial activities, cytotoxicity evaluation, and phytochemical identification by GC-MS. Antibiotics (Basel) 11 (12). https://doi.org/10.3390/antibiotics11121699.
van de Laar, F.A., Lucassen, P.L., Akkermans, R.P., van de Lisdonk, E.H., Rutten, G.E., van Weel, C., 2005a. Alpha-glucosidase inhibitors for patients with type 2 diabetes: results from a Cochrane systematic review and meta-analysis. Diabetes Care 28 (1), 154–163. https://doi.org/10.2337/diacare.28.1.154.
Van de Laar, F.A., Lucassen, P.L., Akkermans, R.P., Van de Lisdonk, E.H., Rutten, G.E., Van Weel, C., 2005b. Alpha-glucosidase inhibitors for type 2 diabetes mellitus. Cochrane Database Syst Rev 2005 (2), Cd003639. https://doi.org/10.1002/14651858.CD003639.pub2.
Wadood, A., Ahmed, N., Shah, L., Ahmad, A., Hassan, H., Shams, S., 2013. In-silico drug design: an approach which revolutionarised the drug discovery process. OA Drug Des. Deliv. 1 (1), 3.
Yan, K.-J., Xu, D.-X., Song, Z.-Q., 2016. Mycetia fangii (Rubiaceae), a new species from South China, with notes on M. cauliflora. Syst. Bot. 41 (1), 229–237. https://doi.org/10.1600/036364416X690624.
Zilani, M.N.H., Uddin, S.J., Hossain, H., Hazni, H., Shilpi, J.A., Hossain, M.G.J.O.P., Medicine, E., 2018. Chemical characterization and bioactivity of Trichosanthes dioica edible shoot extract. Orient Pharm. Exp. Med. 18, 167–175. https://doi.org/10.1007/s13596-018-0310-5.
Zilani, M.N.H., Islam, M.A., Biswas, P., Anisuzzman, M., Hossain, H., Shilpi, J.A., Hasan, M.N., Hossain, M.G., 2021. Metabolite profiling, anti-inflammatory, analgesic potentials of edible herb Colocasia gigantea and molecular docking study against COX-II enzyme. J. Ethnopharmacol. 281, 114577 https://doi.org/10.1016/j.jep.2021.114577.